regulated through c-Fos. NFATc1 activation was partially suppressed, meaning that Jdp2 may also positively regulate its activity. However, we did not detect a direct association between Jdp2 and NFATc1 (data not shown), and Jdp2 had no effect on NFATc1 binding to its promoter region. Thus, indirect mechanisms are likely to modulate the NFATc1 activity.

The defect in osteoclastogenesis in *Jdp2*$^{-/-}$ mice in vivo was relatively mild compared with its effect on in vitro osteoclastogenesis. It has been reported that calcium signaling is important for NFATc1 activation and that such costimulatory signaling is supported by ITAM-harboring adaptors, such as FcRγ and DNAX-activation protein 12 (DAP12) (Koga et al., 2004). Because RANKL-induced calcium oscillation was normal in *Jdp2*$^{-/-}$ cells in this study, signaling through ITAM-harboring molecules is likely to be normal. These findings further suggest that another unknown costimulatory signaling pathway may be compensating for the Jdp2 deficiency in vivo. Further studies are needed to explore the role of Jdp2 in osteoclasts, but our data provide insights into c-Fos-Jdp2 axis-mediated osteoclastogenesis and suggest a basis for the possibility of Jdp2-targeted therapeutic approaches to treat osteoporosis.

Our present data clearly revealed an unexpected and strict requirement for Jdp2 in proper differentiation of neutrophils. *Jdp2*$^{-/-}$ neutrophils were morphologically normal but had impaired surface expression of Ly6G, apoptosis, and bactericidal function. Furthermore, C/EBPα activation and expression of Bcl-2 and primary granule genes were increased. Our data also suggest that Jdp2 suppresses C/EBPα by directly binding to it. Notably, *Jdp2*$^{-/-}$ neutrophils showed normal primary granule protein levels but increased mRNA levels. Similar discrepancies have been reported in several knockout mice. For example, Gfi1-deficient neutrophils exhibit immature morphology and significant increases in mRNAs, such as primary granule genes and C/EBPα, but lack granules (Hock et al., 2003). Meanwhile, Ikaros-deficient neutrophils have impaired Ly6G levels but normal granule and nuclear morphology, whereas secondary granule mRNAs seem to be increased (Dumortier et al., 2003). Thus, increased mRNA levels of granule genes can be considered a leading indicator for obstruction of differentiation. Unfortunately, we cannot explain why the granule mRNA and protein levels are dissociated in neutrophils. One hypothetical explanation is that there are insufficient amounts of translational components for granule synthesis in *Jdp2*$^{-/-}$ neutrophils.

Jdp2 is homologous to ATF3, a negative regulator of TLR signaling, and ATF3 expression is suppressed by Jdp2 in fibroblasts (Weidenfeld-Baranboim et al., 2009). Our genome-wide analysis revealed that the ATF3 promoter region was highly acetylated in *Jdp2*$^{-/-}$ neutrophils. Furthermore, we discovered that Jdp2 directly binds to the ATF3 promoter in neutrophils. Importantly, ATF3 may function as a novel negative regulator of Ly6G. We also revealed that *Jdp2*$^{-/-}$ mice are highly susceptible to infection. The impaired NET formation and ROS production in *Jdp2*$^{-/-}$ neutrophils may be responsible for the increased susceptibility to infection in *Jdp2*$^{-/-}$ mice. Intriguingly, this defect in the in vitro bactericidal function of *Jdp2*$^{-/-}$ neutrophils was mild compared with the highly impaired resistance to *S. aureus* infection. We cannot completely exclude the possibility of defects in other immune cells. Thus, our data suggest the importance of Jdp2 in host defense and also enhance curiosity to clarify the importance of Jdp2 in a wide range of hematopoietic cell functions.

Taken together, we have identified Jdp2 as a critical "osteo-innate-immunological" regulator both in vivo and in vitro. Thus, Jdp2-mediated gene regulation may be a critical target for the development of therapeutics to control abnormal neutrophil- and osteoclast-associated diseases.

EXPERIMENTAL PROCEDURES

Mice, Cells, and Reagents

The generation of *Jdp2*$^{-/-}$ mice is described in the Supplemental Experimental Procedures. Mice were housed in specific-pathogen-free conditions and all animal experiments were carried out with the approval of the animal research committee of the Research Institute for Microbial Diseases (Osaka University). Peritoneal neutrophils were prepared as described (Bertram et al., 2012). B and T cells were isolated from splenocytes with anti-B220 and anti-Thy-1.2 magnetic beads (Miltenyi Biotec), respectively. Splenic dendritic cells (DCs) were isolated with anti-CD11c magnetic beads (Miltenyi Biotec). Primary osteoclasts are prepared as described (Takegahara et al., 2006). Splenic- or bone marrow-derived CD11b^{+}F4/80^{+} macrophages and CD11b^{+}Ly6C^{lo}Ly6G^{+} neutrophils were sorted with a FACSAria (BD Biosciences). Conventional dendritic cells (cDCs) were prepared as described (Kato et al., 2005). *S. aureus* 834 was kindly provided by A. Nakane (Hirosaki University, School of Medicine, Aomori, Japan). This strain was cultured on tryptic soy broth agar plates at 37°C for 24 hr before use. *C. albicans* THK519 was obtained from a patient admitted to Tohoku University Hospital (Sendai, Japan). These cells were cultured on potato dextrose agar (PDA) plates (Eiken) at 30°C for 72 hr before use. The pathogen-associated molecular patterns (PAMPs), Abs, and ELISA kits listed in the Supplemental Experimental Procedures were purchased. Phagocytosis was quantified with a phagocytosis assay kit (500290; Cayman Chemical Company). Superoxide and apoptosis levels were measured with a Diogenes Cellular Luminescence Enhancement System (National Diagnostics) and annexin V-indocarbocyanine (BioVision), respectively.

Analysis of Osteoclastogenesis and Bone Phenotype

For in vitro osteoclast culture, MDMs were generated as described (Maruyama et al., 2006). MDMs were induced to differentiate into osteoclasts in the presence of 25 ng/ml M-CSF and various concentrations of RANKL (R&D Systems). After 3 days, TRAP staining was performed as described (Zhao et al., 2006). For pit assays, MDMs were cultured on bone resorption assay plates (Iwai Chemical Company) with 50 ng/ml RANKL. After 5 days, the plates were immersed in 1 M NH_4OH for 3 hr, and the resorption pits were counted. The in vivo bone phenotype was analyzed as described in the Supplemental Experimental Procedures.

Bone Marrow Transfer

Bone marrow transplantation was performed as described in the Supplemental Experimental Procedures.

qPCR

RNA was extracted from cells with TRIzol (Invitrogen Life Science Technologies), and reverse transcription was performed with ReverTra Ace (Toyobo Co. Ltd.). qPCR was performed in an ABI PRISM 7500 with TaqMan Assay-on-demand primers (Applied Biosystems).

Viral Gene Transfer and RNA Interference

Retroviral or lentiviral gene transfer was performed as described in the Supplemental Experimental Procedures. A siRNA for c-Fos (Stealth RNAi siRNA, MSS247212; Invitrogen) and a control oligo (Stealth RNAi siRNA, negative control Med GC; Invitrogen) were introduced into MDMs with Lipofectamine 2000 (Invitrogen) according to the manufacturer's protocols.

Immunoblotting and Immunoprecipitation

Immunoblotting and immunoprecipitation were performed as described (Kawagoe et al., 2009).

Luciferase Reporter Assay

A *C/EBP* reporter kit (*CCS-001L*; *QIAGEN*) and *NFAT* reporter kit (*CCS-015L*; QIAGEN) were used for transient transfection into HEK293 cells with Lipofectamine 2000. Luciferase activities were measured with a Dual-Luciferase Reporter Assay System (Promega), as described (Iwasaki et al., 2011).

Intracellular Calcium Imaging

MDMs were plated on poly-L-lysine-coated glass-bottom dishes and loaded with 5 μM Fura-2/AM for 30 min in loading solution (115 mM NaCl, 5.4 mM KCl, 1 mM $MgCl_2$, 2 mM $CaCl_2$, 20 mM HEPES, 10 mM glucose [pH 7.42]). Fura-2 fluorescent images were analyzed as described (Kuroda et al., 2008).

Immunostaining, FACS, and TEM

Immunostaining of in vitro cultured peritoneal neutrophils was performed essentially as described (Li et al., 2010). Peritoneal neutrophils were stimulated by *S. aureus* or *C. albicans* for 2 hr (MOI = 50) and stained with Hoechst and anti-histone H3 Cit3 Ab (Abcam). Abs for FACS were purchased from BD Biosciences and used for cell staining. Data were acquired in a FACSCalibur (BD Biosciences) and analyzed with FlowJo (Ashland). TEM was performed as described in the Supplemental Experimental Procedures.

Colony Assay

Bone marrow cells were cultured with MethoCult (GFM3434; Stem Cell Technologies) with or without G-CSF (50 ng/ml) supplementation, according to the manufacturer's protocol. After 7 days, the numbers of CFU-G, CFU-M, and CFU-GM were counted.

Microarray, ChIP, and ChIP-seq Analyses

The microarray, ChIP, and ChIP-seq protocols and data analyses are described in the Supplemental Experimental Procedures.

In Vitro and In Vivo Infection

In vitro bacterial killing assays were performed as described in the Supplemental Experimental Procedures. For in vivo infection, *S. aureus* was cultured in tryptic soy broth for 15 hr at 37°C. Cells were collected and suspended in PBS. Mice were infected intravenously with 0.2 ml of solution containing 3×10^7 *S. aureus* cells. *C. albicans* were collected from PDA plates and suspended in PBS. Mice were infected intravenously with 0.2 ml of solution containing 2.5×10^5 *C. albicans* cells. The numbers of viable bacteria in various organs were determined as described (Maruyama et al., 2007).

Statistical Analysis

Student's t test was used to evaluate the significance of differences, with significance set at $p < 0.05$. For survival curves, two groups were compared with a log-rank test.

ACCESSION NUMBERS

The microarray data are available in the Gene Expression Omnibus (GEO) database (http://www.ncbi.nlm.nih.gov/gds) under the accession number GSE42063.

SUPPLEMENTAL INFORMATION

Supplemental Information includes Supplemental Experimental Procedures, six figures, and one table and can be found with this article online at http://dx.doi.org/10.1016/j.immuni.2012.08.022.

ACKNOWLEDGMENTS

We thank S. Tartey and D. Ori for technical advice; E. Kamada and M. Kageyama for secretarial assistance; K. Nojima, Y. Fujiwara, and M. Kumagai for technical assistance; and T. Kawai and Y. Kumagai for fruitful discussions. This work was supported by Special Coordination Funds of the Japanese Ministry of Education, Culture, Sports, Science, and Technology, grants from the Ministry of Health, Labour, and Welfare of Japan, the Japan Society for the Promotion of Science (JSPS) through the Funding Program for World-Leading Innovative R&D on Science and Technology (FIRST Program), and a research fellowship from the JSPS for the Promotion of Science for Young Scientists. K.M. designed and performed most of the experiments. M.F., T.S., T. Kawasaki, T. Kondo, H.K., N.T., and O.T. contributed the immunological experiments. A.V. and D.S. analyzed the ChIP-seq data. K.K.Y. provided the Jdp2 antibody. The manuscript was written by K.M. S.A. supervised the overall research.

Received: May 11, 2012
Accepted: August 16, 2012
Published online: November 29, 2012

REFERENCES

Aronheim, A., Zandi, E., Hennemann, H., Elledge, S.J., and Karin, M. (1997). Isolation of an AP-1 repressor by a novel method for detecting protein-protein interactions. Mol. Cell. Biol. *17*, 3094–3102.

Bertram, A., Zhang, H., von Vietinghoff, S., de Pablo, C., Haller, H., Shushakova, N., and Ley, K. (2012). Protein kinase C-θ is required for murine neutrophil recruitment and adhesion strengthening under flow. J. Immunol. *188*, 4043–4051.

Borregaard, N., and Cowland, J.B. (1997). Granules of the human neutrophilic polymorphonuclear leukocyte. Blood *89*, 3503–3521.

Borregaard, N., Sørensen, O.E., and Theilgaard-Mönch, K. (2007). Neutrophil granules: a library of innate immunity proteins. Trends Immunol. *28*, 340–345.

Brinkmann, V., Reichard, U., Goosmann, C., Fauler, B., Uhlemann, Y., Weiss, D.S., Weinrauch, Y., and Zychlinsky, A. (2004). Neutrophil extracellular traps kill bacteria. Science *303*, 1532–1535.

Colonna, M., Trinchieri, G., and Liu, Y.J. (2004). Plasmacytoid dendritic cells in immunity. Nat. Immunol. *5*, 1219–1226.

Dumortier, A., Kirstetter, P., Kastner, P., and Chan, S. (2003). Ikaros regulates neutrophil differentiation. Blood *101*, 2219–2226.

Forman, H.J., and Thomas, M.J. (1986). Oxidant production and bactericidal activity of phagocytes. Annu. Rev. Physiol. *48*, 669–680.

Hestdal, K., Ruscetti, F.W., Ihle, J.N., Jacobsen, S.E., Dubois, C.M., Kopp, W.C., Longo, D.L., and Keller, J.R. (1991). Characterization and regulation of RB6-8C5 antigen expression on murine bone marrow cells. J. Immunol. *147*, 22–28.

Hock, H., Hamblen, M.J., Rooke, H.M., Traver, D., Bronson, R.T., Cameron, S., and Orkin, S.H. (2003). Intrinsic requirement for zinc finger transcription factor Gfi-1 in neutrophil differentiation. Immunity *18*, 109–120.

Huang, Y.C., Saito, S., and Yokoyama, K.K. (2010). Histone chaperone Jun dimerization protein 2 (JDP2): role in cellular senescence and aging. Kaohsiung J. Med. Sci. *26*, 515–531.

Humphrey, M.B., Daws, M.R., Spusta, S.C., Niemi, E.C., Torchia, J.A., Lanier, L.L., Seaman, W.E., and Nakamura, M.C. (2006). TREM2, a DAP12-associated receptor, regulates osteoclast differentiation and function. J. Bone Miner. Res. *21*, 237–245.

Iwasaki, H., Takeuchi, O., Teraguchi, S., Matsushita, K., Uehata, T., Kuniyoshi, K., Satoh, T., Saitoh, T., Matsushita, M., Standley, D.M., and Akira, S. (2011). The IκB kinase complex regulates the stability of cytokine-encoding mRNA induced by TLR-IL-1R by controlling degradation of regnase-1. Nat. Immunol. *12*, 1167–1175.

Ji, H., Ehrlich, L.I., Seita, J., Murakami, P., Doi, A., Lindau, P., Lee, H., Aryee, M.J., Irizarry, R.A., Kim, K., et al. (2010). Comprehensive methylome map of lineage commitment from haematopoietic progenitors. Nature *467*, 338–342.

Jin, C., Ugai, H., Song, J., Murata, T., Nili, F., Sun, K., Horikoshi, M., and Yokoyama, K.K. (2001). Identification of mouse Jun dimerization protein 2 as a novel repressor of ATF-2. FEBS Lett. *489*, 34–41.

Jin, C., Kato, K., Chimura, T., Yamasaki, T., Nakade, K., Murata, T., Li, H., Pan, J., Zhao, M., Sun, K., et al. (2006). Regulation of histone acetylation and nucleosome assembly by transcription factor JDP2. Nat. Struct. Mol. Biol. *13*, 331–338.

Karsenty, G., and Wagner, E.F. (2002). Reaching a genetic and molecular understanding of skeletal development. Dev. Cell *2*, 389–406.

Kato, H., Sato, S., Yoneyama, M., Yamamoto, M., Uematsu, S., Matsui, K., Tsujimura, T., Takeda, K., Fujita, T., Takeuchi, O., and Akira, S. (2005). Cell type-specific involvement of RIG-I in antiviral response. Immunity *23*, 19–28.

Kawagoe, T., Takeuchi, O., Takabatake, Y., Kato, H., Isaka, Y., Tsujimura, T., and Akira, S. (2009). TANK is a negative regulator of Toll-like receptor signaling and is critical for the prevention of autoimmune nephritis. Nat. Immunol. *10*, 965–972.

Kawaida, R., Ohtsuka, T., Okutsu, J., Takahashi, T., Kadono, Y., Oda, H., Hikita, A., Nakamura, K., Tanaka, S., and Furukawa, H. (2003). Jun dimerization protein 2 (JDP2), a member of the AP-1 family of transcription factor, mediates osteoclast differentiation induced by RANKL. J. Exp. Med. *197*, 1029–1035.

Koga, T., Inui, M., Inoue, K., Kim, S., Suematsu, A., Kobayashi, E., Iwata, T., Ohnishi, H., Matozaki, T., Kodama, T., et al. (2004). Costimulatory signals mediated by the ITAM motif cooperate with RANKL for bone homeostasis. Nature *428*, 758–763.

Kuroda, Y., Hisatsune, C., Nakamura, T., Matsuo, K., and Mikoshiba, K. (2008). Osteoblasts induce Ca2+ oscillation-independent NFATc1 activation during osteoclastogenesis. Proc. Natl. Acad. Sci. USA *105*, 8643–8648.

Lagasse, E., and Weissman, I.L. (1996). Flow cytometric identification of murine neutrophils and monocytes. J. Immunol. Methods *197*, 139–150.

Li, P., Li, M., Lindberg, M.R., Kennett, M.J., Xiong, N., and Wang, Y. (2010). PAD4 is essential for antibacterial innate immunity mediated by neutrophil extracellular traps. J. Exp. Med. *207*, 1853–1862.

Lieschke, G.J., Grail, D., Hodgson, G., Metcalf, D., Stanley, E., Cheers, C., Fowler, K.J., Basu, S., Zhan, Y.F., and Dunn, A.R. (1994). Mice lacking granulocyte colony-stimulating factor have chronic neutropenia, granulocyte and macrophage progenitor cell deficiency, and impaired neutrophil mobilization. Blood *84*, 1737–1746.

Martinelli, S., Urosevic, M., Daryadel, A., Oberholzer, P.A., Baumann, C., Fey, M.F., Dummer, R., Simon, H.U., and Yousefi, S. (2004). Induction of genes mediating interferon-dependent extracellular trap formation during neutrophil differentiation. J. Biol. Chem. *279*, 44123–44132.

Maruyama, K., Takada, Y., Ray, N., Kishimoto, Y., Penninger, J.M., Yasuda, H., and Matsuo, K. (2006). Receptor activator of NF-kappa B ligand and osteoprotegerin regulate proinflammatory cytokine production in mice. J. Immunol. *177*, 3799–3805.

Maruyama, K., Sano, G., Ray, N., Takada, Y., and Matsuo, K. (2007). c-Fos-deficient mice are susceptible to *Salmonella enterica serovar Typhimurium* infection. Infect. Immun. *75*, 1520–1523.

Nishikawa, K., Nakashima, T., Hayashi, M., Fukunaga, T., Kato, S., Kodama, T., Takahashi, S., Calame, K., and Takayanagi, H. (2010). Blimp1-mediated repression of negative regulators is required for osteoclast differentiation. Proc. Natl. Acad. Sci. USA *107*, 3117–3122.

Nishinaka, Y., Arai, T., Adachi, S., Takaori-Kondo, A., and Yamashita, K. (2011). Singlet oxygen is essential for neutrophil extracellular trap formation. Biochem. Biophys. Res. Commun. *413*, 75–79.

Takayanagi, H. (2007). Osteoimmunology: shared mechanisms and crosstalk between the immune and bone systems. Nat. Rev. Immunol. *7*, 292–304.

Takegahara, N., Takamatsu, H., Toyofuku, T., Tsujimura, T., Okuno, T., Yukawa, K., Mizui, M., Yamamoto, M., Prasad, D.V., Suzuki, K., et al. (2006). Plexin-A1 and its interaction with DAP12 in immune responses and bone homeostasis. Nat. Cell Biol. *8*, 615–622.

Weidenfeld-Baranboim, K., Hasin, T., Darlyuk, I., Heinrich, R., Elhanani, O., Pan, J., Yokoyama, K.K., and Aronheim, A. (2009). The ubiquitously expressed bZIP inhibitor, JDP2, suppresses the transcription of its homologue immediate early gene counterpart, ATF3. Nucleic Acids Res. *37*, 2194–2203.

Yamanaka, R., Barlow, C., Lekstrom-Himes, J., Castilla, L.H., Liu, P.P., Eckhaus, M., Decker, T., Wynshaw-Boris, A., and Xanthopoulos, K.G. (1997). Impaired granulopoiesis, myelodysplasia, and early lethality in CCAAT/enhancer binding protein epsilon-deficient mice. Proc. Natl. Acad. Sci. USA *94*, 13187–13192.

Zhang, P., Iwama, A., Datta, M.W., Darlington, G.J., Link, D.C., and Tenen, D.G. (1998). Upregulation of interleukin 6 and granulocyte colony-stimulating factor receptors by transcription factor CCAAT enhancer binding protein alpha (C/EBP alpha) is critical for granulopoiesis. J. Exp. Med. *188*, 1173–1184.

Zhao, C., Irie, N., Takada, Y., Shimoda, K., Miyamoto, T., Nishiwaki, T., Suda, T., and Matsuo, K. (2006). Bidirectional ephrinB2-EphB4 signaling controls bone homeostasis. Cell Metab. *4*, 111–121.

THE JOURNAL OF BIOLOGICAL CHEMISTRY VOL. 287, NO. 34, pp. 29114–29124, August 17, 2012

TRAF Family Member-associated NF-κB Activator (TANK) Is a Negative Regulator of Osteoclastogenesis and Bone Formation*[S]

Received for publication, January 30, 2012, and in revised form, June 21, 2012 Published, JBC Papers in Press, July 6, 2012, DOI 10.1074/jbc.M112.347799

Kenta Maruyama[‡], Tatsukata Kawagoe[‡], Takeshi Kondo[‡§], Shizuo Akira[‡§1], and Osamu Takeuchi[‡¶2]

From the [‡]Laboratory of Host Defense, WPI Immunology Frontier Research Center (IFReC), and [§]Research Institute for Microbial Diseases, Osaka University, 3-1 Yamada-oka, Suita, Osaka 565-0871, Japan and the [¶]Institute for Virus Research, Kyoto University, 53 Shogoin Kawara-cho, Sakyo-ku, Kyoto 606-8507, Japan

Background: Osteoclasts and osteoblasts are major players in bone metabolism.
Results: TRAF family member-associated NF-κB activator (TANK) is induced during osteoclastogenesis and osteoblastogenesis. RANKL-induced osteoclastogenesis was increased in TANK-deficient cells. Osteoblastogenesis was also increased in TANK-deficient mice.
Conclusion: TANK is a negative feedback regulator of osteoclastogenesis and osteoblastogenesis.
Significance: TANK is a novel suppressor of bone degradation and formation.

The differentiation of bone-resorbing osteoclasts is induced by RANKL signaling, and leads to the activation of NF-κB via TRAF6 activation. TRAF family member-associated NF-κB activator (TANK) acts as a negative regulator of Toll-like receptors (TLRs) and B-cell receptor (BCR) signaling by inhibiting TRAF6 activation. *Tank*$^{-/-}$ mice spontaneously develop autoimmune glomerular nephritis in an IL-6-dependent manner. Despite its importance in the TCRs and BCR-activated TRAF6 inhibition, the involvement of TANK in RANKL signaling is poorly understood. Here, we report that TANK is a negative regulator of osteoclast differentiation. The expression levels of TANK mRNA and protein were up-regulated during RANKL-induced osteoclastogenesis, and overexpression of TANK *in vitro* led to a decrease in osteoclast formation. The *in vitro* osteoclastogenesis of *Tank*$^{-/-}$ cells was significantly increased, accompanied by increased ubiquitination of TRAF6 and enhanced canonical NF-κB activation in response to RANKL stimulation. *Tank*$^{-/-}$ mice showed severe trabecular bone loss, but increased cortical bone mineral density, because of enhanced bone erosion and formation. TANK mRNA expression was induced during osteoblast differentiation and *Tank*$^{-/-}$ osteoblasts exhibited enhaced NF-κB activation, IL-11 expression, and bone nodule formation than wild-type control cells. Finally, wild-type mice transplanted with bone marrow cells from *Tank*$^{-/-}$ mice showed trabecular bone loss analogous to that in *Tank*$^{-/-}$ mice. These findings demonstrate that TANK is critical for osteoclastogenesis by regulating NF-κB, and is also important for proper bone remodeling.

Bone mass and structure are strictly regulated by the delicate balance between bone resorption and formation. Bone-forming osteoblasts are derived from mesenchymal cells and express M-CSF and receptor activator of NF-κB (RANK)[3] ligand (RANKL). Runt-related transcription factor 2 (Runx2) is known to a key transcription factor for osteoblast differentiation. On the other hand, bone-resorbing osteoclasts are giant, multinucleated, tartrate-resistant acid phosphatase (TRAP)-positive cells derived from the monocyte/macrophage lineage (1). When M-CSF and RANKL stimulate their receptors c-fms and RANK on osteoclast precursors, respectively, transcription factors such as NFATc1 (2), c-Fos (3), and NF-κB (4) are activated in the cells. NFATc1 is the master regulator of osteoclasts, and NF-κB has been implicated in the induction of NFATc1 (5). The RANKL-induced NF-κB pathways include both canonical and non-canonical pathways. The canonical NF-κB pathway activates heterodimers of RelA/p65 and p50, which is generated from the NF-κB1/p105 fragment, while the non-canonical pathway induces processing of the NF-κB2/p100 fragment into active p52. Following the activation of such transcription factors, osteoclast differentiation is induced by the induction of osteoclastic genes, such as TRAP, calcitonin R, and DC-STAMP. Among these osteoclastic genes, DC-STAMP is known to be involved in cell-cell fusion, because osteoclast and IL-3 plus IL-4-induced multinucleated giant cell formation by

* This work was supported by the Special Coordination Funds of the Japanese Ministry of Education, Culture, Sports, Science, and Technology, grants from the Ministry of Health, Labour, and Welfare in Japan, the Japan Society for the Promotion of Science (JSPS) through the Funding Program for World-Leading Innovative R&D on Science and Technology (FIRST Program), and a research fellowship from the JSPS for the Promotion of Science for Young Scientists.
[S] This article contains supplemental Figs. S1–S3.
[1] To whom correspondence may be addressed: Laboratory of Host Defense, WPI Immunology Frontier Research Center, Osaka University, 3-1 Yamada-oka, Suita, Osaka 565-0871, Japan. Tel.: 81-6-6879-8303; Fax: 81-6-6879-8305; E-mail: sakira@biken.osaka-u.ac.jp.
[2] To whom correspondence may be addressed: Laboratory of Host Defense, WPI Immunology Frontier Research Center, Osaka University, 3-1 Yamada-oka, Suita, Osaka 565-0871, Japan. Tel.: 81-6-6879-8303; Fax: 81-6-6879-8305; E-mail: otake@biken.osaka-u.ac.jp.

[3] The abbreviations used are: RANK, receptor activator of NF-κB; OPG, osteoprotegerin; MDMs, M-CSF-derived macrophages; μCT, microcomputed tomography; TRAP, tartrate-resistant acid phosphatase; BMD, bone mineral density; ALP, alkaline phosphatase; Runx2, runt-related transcription factor 2; TANK, TRAF family-associated NF-κB activator; SHIP, Src homology 2-containing inositol-5-phosphatase.

macrophage cell fusion is abrogated in DC-STAMP-deficient mice (6, 7). Mice lacking both NF-κB1 and NF-κB2 develop typical osteopetrosis through defective development of osteoclasts (8), thereby confirming the importance of NF-κB signaling in controlling bone homeostasis.

RANKL is a major NF-κB activator in osteoclastogenesis. RANKL binds to its receptor RANK, which belongs to the TNF receptor superfamily. Upon activation, RANK recruits TRAF family E3 ubiquitin ligases, such as TRAF2, TRAF5, and TRAF6 (9). Among the TRAF family members, TRAF6 plays a critical role in RANK signaling toward NF-κB, because its deficiency leads to severe osteopetrosis similar to that in RANKL- and RANK-deficient mice (10–12). Collectively, it has been proposed that RANKL-RANK interactions and the subsequent signaling via TRAF6 are important for the differentiation of osteoclasts.

Various cytokines and cellular stresses are known to activate intracellular signaling pathways leading to NF-κB activation. This transcription factor is well known to control the expressions of proinflammatory cytokines downstream of Toll-like receptors (TLRs) and IL-1 receptor (IL-1R). TLRs directly sense the presence of microbial components and trigger intracellular signaling pathways that evoke innate immune responses against pathogens. Activation of TLRs leads to the recruitment of the adaptor molecule MyD88, which in turn activates IL-1R-associated kinases (IRAKs). TRAF6 is ubiquitinated downstream of IRAK-1/-2, and activates NF-κB by generating unconjugated polyubiquitin chains and activating TAK1 (13, 14). The importance of TRAF6 in TLR/IL-1R signaling has been established by the observation that NF-κB activation in response to LPS and IL-1 fails in TRAF6-deficient mice (11). In acquired immunity, the antigen receptor signaling pathways emanating from TCR and BCR are known to activate NF-κB via TRAF proteins.

TRAF family member-associated NF-κB activator (TANK; also known as TRAF-interacting protein) binds to TRAF1, TRAF2, TRAF3, TRAF5, and TRAF6 (15–18), and acts as a regulator of TRAF-mediated signaling. Macrophages and B cells from TANK-deficient ($Tank^{-/-}$) mice exhibit more enhanced NF-κB and AP-1 activation in response to stimulation of TLRs and B-cell receptor (BCR) (19). TLR and BCR-induced ubiquitination of TRAF6 is up-regulated in $Tank^{-/-}$ macrophages, suggesting that TANK inhibits TRAF6 activation downstream of TLRs (19). While TANK has been implicated in the type I IFN responses against virus infection by binding to TANK-binding kinase 1 (20), type I IFNs are produced normally in $Tank^{-/-}$ cells in response to RNA virus infection (19). Furthermore, $Tank^{-/-}$ mice spontaneously develop lupus-like autoimmune nephritis through IL-6 expression (19). MyD88 and the intestinal flora contribute to the development of autoantibody production in $Tank^{-/-}$ mice (19), suggesting that spontaneous activation of TLRs by intestinal bacteria leads to IL-6 production that causes autoimmunity.

Despite the importance of TRAF6 in the RANKL signaling, the involvement of TANK in RANKL-induced osteoclast differentiation and bone homeostasis is poorly understood. In this study, we found that TANK was induced during RANKL-mediated osteoclastogenesis, and overexpression of TANK led to a decrease in osteoclast formation. $Tank^{-/-}$ macrophages underwent increased osteoclastogenesis mediated by enhanced ubiquitination of TRAF6, the canonical NF-κB pathway, and c-Fos and NFATc1 activation. $Tank^{-/-}$ mice showed trabecular bone loss, but increased cortical bone mineral density (BMD) and resistance to bone fracture, because of enhanced bone erosion and formation. Interestingly, TANK was also induced in osteoblasts and $Tank^{-/-}$ osteoblasts formed more bone nodules. These findings provide unexpected insights into the roles of TANK in bone remodeling.

EXPERIMENTAL PROCEDURES

Mice—$Tank^{-/-}$ mice on a C57BL/6 background were generated as previously described (19) and maintained under specific pathogen-free conditions. All animal experiments were carried out under approval from the Animal Research Committee of the Research Institute for Microbial Diseases (Osaka University, Osaka, Japan).

In Vitro Osteoclast Culture and Functional Evaluation—For stromal cell-free *in vitro* osteoclast cultures, M-CSF-derived macrophages (MDMs) were used as osteoclast precursors. Bone marrow cells were flushed from femurs or tibias and cultured for 6 h in α-MEM containing 10% FCS. Non-adherent cells were collected and plated in 48-well plates at a density of 1.2×10^5 cells/well with 25 ng/ml M-CSF (PeproTech, Rocky Hill, NJ). After 3 days, the cultures were washed with PBS and adherent cells were used as MDMs. The MDMs were induced to differentiate into osteoclasts in the presence of 25 ng/ml M-CSF and various concentrations of RANKL (R&D Systems, Minneapolis, MN). After 3 days, the adherent cells were fixed with 4% paraformaldehyde, treated with ethanol/acetone (50:50, v/v), and stained for TRAP using a TRAP/ALP staining kit (Wako, Tokyo, Japan). The numbers of TRAP-positive multinucleated cells were counted. The osteoclast area (percentage of TRAP-positive multinucleated cells relative to the total area) was measured using the software ImageJ (software from NIH). For pit assays, ivory dentine slices (Wako, Tokyo, Japan) were placed in 48-well plates. MDMs were cultured on the dentine slices, and then cultured in 25 ng/ml M-CSF and 50 ng/ml RANKL to induce osteoclast differentiation. After 5 days, the dentine slices were immersed in 1 M NH_4OH for 3 h and sonicated to remove the cells. The resorption pits were observed by scanning electron microscopy (MiniScope TM-1000; Hitachi, Tokyo, Japan). Quantitative analyses of the resorption pits were performed using ImageJ.

Retroviral Gene Transfer—A murine TANK cDNA was cloned into the pLZR-IRES/GFP retroviral vector (21). The construct was transfected into the packaging cell line PlatE, and viral supernatants were collected. Bone marrow cells from C57BL/6 mice were cultured for 6 h in α-MEM. Subsequently, non-adherent cells were collected and plated in 24-well plates at a density of 1×10^6 cells/well with 25 ng/ml M-CSF. After 24 h, the cells were transduced with a retroviral supernatant in the presence of 8 μg/ml polybrene for 8 h. Following culture for 48 h in the presence of 25 ng/ml M-CSF, the cells were cultured with 25 ng/ml M-CSF and 50 ng/ml RANKL. After 3 days, the numbers of TRAP-positive multinucleated cells were counted.

Immunoblotting, Immunoprecipitation, and Ubiquitination Assays—MDMs (5×10^6) were stimulated with 50 ng/ml LPS, TNF-α, or RANKL for various times. The cells were then lysed in a lysis buffer comprising 20 mM Tris-HCl, 1 mM EDTA, 1.0% Nonidet P40, 150 mM NaCl, and a protease inhibitor mixture (Roche Diagnostics, Mannheim, Germany). The cell lysates were separated by SDS-PAGE and transferred onto polyvinylfluoride membranes. The membranes were incubated with anti-TANK (H-300; Santa Cruz Biotechnology, Santa Cruz, CA), anti-p100/p52 (#4882; Cell Signaling), anti-TRAF6 (sc-7221; Santa Cruz Biotechnology), anti-Ub (P4D1; Santa Cruz Biotechnology), and anti-actin (C-11; Santa Cruz Biotechnology) antibodies. After the incubation, membranes were washed and incubated with HRP-linked anti-rabbit IgG (NA934V; GE Healthcare) or HRP-linked anti-mouse IgG (NA931V; GE Healthcare). For chemiluminescence, membranes were incubated with fresh Western lightning Plus-ECL reagents (Perkin Elmer). TRAF6 immunoprecipitation and detection of its ubiquitination were performed as described previously (19).

Proliferation and Apoptosis Assays—Cells from wild-type and *Tank*$^{-/-}$ mice were stained with trypan blue, and the numbers of viable cells were counted under a light microscope. Apoptotic cells were determined using a Poly Caspase Assay Kit, Green FLICA (ImmunoChemistry Technologies, Bloomington, MN).

DNA Binding Activity of NF-κB p65—MDMs (1×10^6) were stimulated with 350 ng/ml RANKL for 30 min. Nuclear extracts were purified from the cells and the DNA binding activity of NF-κB p65 was analyzed using a TransAM Transcription Factor Assay Kit (Active Motive, Carlsbad, CA).

Osteoblast Culture and Functional Assays—Primary osteoblasts were isolated from the calvariae of 2-day-old mice. The calvariae were digested in α-MEM containing 0.1% collagenase and 0.2% dispase at 37 °C for 10 min. The cells were then expanded in α-MEM containing 10% FCS. For induction of osteoblastogenesis, primary osteoblasts were plated in 48-well plates at a density of 3×10^4 cells/well. After 1 day, the medium was supplemented with an Osteoblast-Inducer Reagent (Takara, Tokyo, Japan) containing ascorbic acid, hydrocortisone, and glycerophosphate. In some experiment, 10 μg/ml neutralizing antibodies to IL-6 or IL-11 (R&D) were added to the medium. The medium was changed every 3 days. After 9 days, calcified nodules and ALP were stained using a Calcified nodule Staining kit (AK-21; Primary Cell, Hokkaido, Japan) and TRAP/ALP staining kit (Wako, Tokyo, Japan), respectively. In some experiments, 5 mM NF-κB inhibitor BAY117085 (Sigma) was added at day 9 for 24 h, and mRNA was harvested.

Osteoclast and Osteoblast Coculture—Bone marrow cells (3×10^5) and primary calvarial osteoblasts (5×10^5) were isolated and cultured in 24-well plates containing α-MEM supplemented with 10% FCS for 10 days in the presence of 10 nM $1\alpha,25(OH)_2D_3$. After the culture, the cells were fixed and stained for TRAP to evaluate the numbers of osteoclasts.

Quantitative PCR Analysis—RNA was extracted from cultured cells using TRIzol (Invitrogen, Carlsbad, CA) and subjected to reverse transcription using ReverTra Ace (Toyobo, Tokyo, Japan). Quantitative PCR was performed with an ABI PRISM 7500 using TaqMan Assays-on-Demand primers and probes (Applied Biosystems) for TANK, TRAP, calcitonin R, c-Fos, NFATc1, DC-STAMP, RANK, Runx2, IL-11, OncostatinM, IL-6, RANKL, and osteoprotegerin (OPG). 18S control reagents were used for normalization of the cDNAs.

Bone Phenotype Analyses—Double calcein labeling was carried out to measure bone formation. Ten-week-old *Tank*$^{-/-}$ and age-matched control wild-type female mice were administered calcein intraperitoneally at 16 mg/kg body weight at 4 and 1 days before euthanasia. After euthanasia, the femurs are removed, fixed with 70% ethanol, and subjected to histomorphometric analyses. Three-dimensional μCT analysis of the femurs was conducted using Scan-Xmate RB080SS110 (Comscan Techno Co. Ltd., Kanagawa, Japan) and TRI/3D-Bon (Ratoc System Engineering Co. Ltd., Tokyo, Japan) software. The cortical BMD and cortical area were measured by Dual Energy x-ray Absorptiometry DCS-600EX-IIIR (Aloka, Tokyo, Japan). To evaluate the cortical bone mechanical properties, the right femoral mid-shaft was tested by three-point bending using a mechanical testing machine (MZ-500S; Maruto, Tokyo, Japan). To test the bone mechanical properties, each femur was placed on two lower supports that were 6 mm apart and tested with a displacement rate of 2 mm/min until failure. The whole bone mechanical properties of maximum load (N), stiffness (N/mm), post-yield deflection (mm), and work to failure (N.mm) were measured. The bone microarchitectural parameters were analyzed in the trabecular regions from 0.1 to 1.5 mm away from the chondro-osseous junction. For bone histomorphometric analyses, the tibias or femurs were fixed with 70% ethanol, subjected to Villanueva bone staining, and embedded in methyl methacrylate. Serial longitudinal sections (6 mm in thickness) of proximal tibias and cross sections of proximal one-third of the right shaft of femurs were prepared using an RM2255 microtome (Leica, Jena, Germany). Metaphysis areas of tibias and endosteum/periosteum areas of femurs were analyzed using a Histometry RT Camera (System Supply Co. Ltd., Nagano, Japan).

Generation of Bone Marrow Chimeric Mice—Donor bone marrow cells were collected from 6-week-old *Tank*$^{-/-}$ and age-matched control wild-type female mice. After suspension in PBS, 1×10^7 cells were intravenously injected into lethally irradiated 4-week-old wild-type recipient mice (C57BL/6 background). The chimeric mice were given neomycin and ampicillin in their drinking water for 4 weeks. The mice were analyzed at 7 weeks after the bone marrow transplantation.

ALP Activity Assay—Cultured calvarial osteoblasts were homogenized with 0.1% Triton X-100, and the alkaline phosphatase (ALP) activity was measured using a kit (LabAssay; Wako). The serum ALP levels were also measured using the same kit.

ELISA—The serum levels of TRACP5b were measured using a TRACP5b ELISA Kit (Immunodiagnostic Systems, Bolden, UK). Serum levels of Cross Linked C-Telopeptide of Type I collagen (CTX-I) were measured by ELISA Kit (USCN Life Science, Wuhan, China). All assays were performed according to the corresponding manufacturer's protocols.

Statistical Analysis—The significance of differences between values was analyzed by Student's *t* test. Values of $p < 0.05$ were accepted as statistically significant.

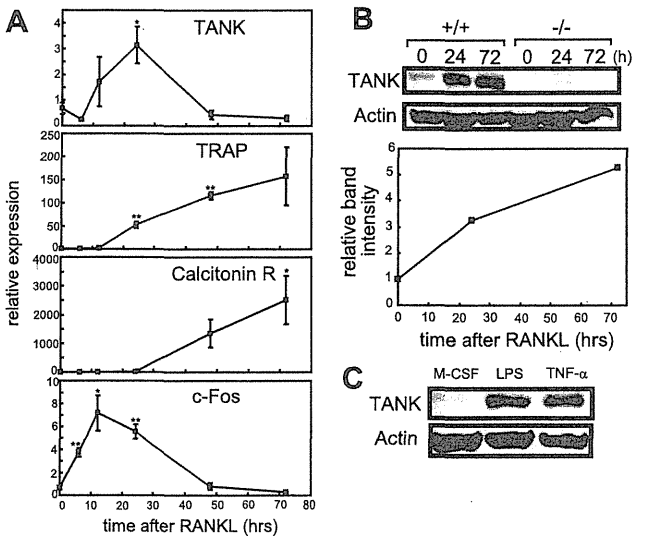

FIGURE 1. **TANK is induced by RANKL.** *A*, MDMs from wild-type mice were treated with M-CSF plus 25 ng/ml RANKL for 0, 6, 12, 24, 48, and 72 h. The mRNA levels of TANK and osteoclastogenic markers such as TRAP, Calcitonin receptor (Calcitonin R), and c-Fos were measured by quantitative PCR. Error bars: S.E. ($n = 3$). *, $p < 0.05$, **, $p < 0.01$, *versus* 0 h. *B*, MDMs from wild-type and *Tank*$^{-/-}$ mice were treated with M-CSF alone (0 h) or 50 ng/ml RANKL plus M-CSF (24 and 72 h) and the levels of TANK expression were analyzed by Western blotting. The relative band intensities of wild-type MDMs were measured using ImageJ and normalized by actin expression. *C*, MDMs from wild-type and *Tank*$^{-/-}$ mice were treated with M-CSF alone (M-CSF), 50 ng/ml LPS plus M-CSF (LPS), or 50 ng/ml TNF-α plus M-CSF for 24 h and the levels of TANK expression was analyzed by Western blotting. The data shown are representative of three independent experiments.

RESULTS

TANK Expression Is Induced by RANKL Stimulation—First, we examined the expression pattern of TANK during the course of RANKL-induced osteoclastogenesis. TANK mRNA expression was markedly increased after 24 h of RANKL stimulation in MDMs, and then decreased to the pre-stimulation level by 48 h of RANKL treatment (Fig. 1*A*). TANK protein expression gradually increased during osteoclastogenesis, and its expression level reached nearly 5-fold after 72 h of RANKL stimulation (Fig. 1*B*). Furthermore, not only RANKL but also LPS and TNF induced TANK expression in MDMs (Fig. 1*C*). These findings prompted us to explore the role of TANK during osteoclastogenesis.

Increased Osteoclast Differentiation and Bone Resorption Activity in Tank$^{-/-}$ *MDMs*—To investigate the role of TANK deficiency in osteoclastogenesis, we analyzed *in vitro* osteoclastogenesis using wild-type and *Tank*$^{-/-}$ MDMs. We treated the MDMs with increasing concentrations of RANKL, and TRAP-positive multinucleated cells were identified as mature osteoclasts after 3 days. RANKL-induced osteoclastogenesis was augmented in *Tank*$^{-/-}$ cells compared with wild-type cells, and the number of osteoclasts was increased by ~60%. Furthermore, *Tank*$^{-/-}$ osteoclasts had increased numbers of nuclei and were larger in size (Fig. 2, *A–D*). TANK deficiency did not alter the proliferation or apoptosis of MDMs (Fig. 2, *F* and *G*).

Next, we compared the bone resorption activities of osteoclasts from wild-type and *Tank*$^{-/-}$ MDMs using pit assays. When wild-type and *Tank*$^{-/-}$ MDMs were cultured on dentine slices with RANKL for 5 days, they formed resorption pits. However, the total bone resorption pit area for *Tank*$^{-/-}$ osteoclasts normalized by osteoclast number was greater than that for wild-type MDMs (Fig. 2*E*), indicating that TANK inhibits the bone resorption activity of bone marrow-derived osteoclasts.

To further substantiate the effect of TANK deficiency on osteoclastogenesis, we examined the expression levels of mRNAs encoding osteoclast-related genes after 0, 24, and 72 h of RANKL stimulation. Consistent with the findings for osteoclastogenesis, the expression profiles revealed that osteoclast-associated genes, including NFATc1, c-Fos, TRAP, calcitonin R, and DC-STAMP, were significantly increased in *Tank*$^{-/-}$ cells compared with wild-type cells (Fig. 3, *A–E*). Collectively, these findings suggest that TANK negatively regulates osteoclast differentiation in cultured bone marrow cells.

TANK Negatively Regulates RANKL Signaling—To explore the effect of gain of function of TANK in osteoclastogenesis, we overexpressed TANK in MDMs using a retroviral vector. As shown in Fig. 4*A*, wild-type MDMs overexpressing TANK did not sufficiently differentiate into osteoclasts, and the number of TRAP-positive multinucleated cells (Fig. 4, *A* and *B*). Further, retrovirus reconstitution of TANK in *Tank*$^{-/-}$ MDMs suppressed RANKL induced osteoclastogenesis to the same level as wild-type (Fig. 4, *A* and *B*). These findings indicate that the level of TANK expression is negatively correlated with osteoclastogenesis induced by RANKL treatment.

To rule out the possibility that differential RANK expression is responsible for the augmented osteoclastogenesis under TANK deficiency, we examined the levels of RANK in MDMs. As shown in Fig. 4*C*, the RANK mRNA levels were comparable between wild-type and *Tank*$^{-/-}$ MDMs. FACS analyses revealed that the RANK^{+}CD11b^{+} osteoclast precursor cell populations in the spleen were also comparable between wild-type and *Tank*$^{-/-}$ mice (supplemental Fig. S1). Next, we checked whether the loss of TANK promoted TRAF6 ubiquitination and NF-κB pathway activation in response to RANKL stimulation. TRAF6 ubiquitination in response to RANKL stimulation was increased in *Tank*$^{-/-}$ MDMs compared with wild-type controls (Fig. 4*D*). Furthermore, RANKL-induced DNA binding of the NF-κB p65 subunit was significantly elevated in *Tank*$^{-/-}$ MDMs (Fig. 4*E*). In contrast, p100 cleavage to p52, which indicates activation of the non-canonical NF-κB pathway, did not differ between wild-type and *Tank*$^{-/-}$ MDMs (Fig. 4*F*). These findings indicate that TANK negatively affects the RANKL-mediated canonical NF-κB pathway by suppressing TRAF6 activation. TANK may act as a negative feedback regulator of osteoclastogenesis.

Tank$^{-/-}$ *Mice Exhibit Increased Cortical BMD and Severe Trabecular Bone Loss*—Next, we analyzed the *in vivo* bone phenotypes of wild-type and *Tank*$^{-/-}$ mice by μCT. First, we investigated the proximal femurs, and found no differences in the bone structures (Fig. 5*A*). However, the cortical area in the mid-shaft of the femurs was slightly increased in *Tank*$^{-/-}$ mice (Fig. 5*B*). This finding was further supported by increased BMD in the proximal end to mid-shaft in the femurs from *Tank*$^{-/-}$ mice (Fig. 5*C*). To determine whether the differences in BMD influenced the mechanical strength of the femur, we performed a three-point bending test on the shaft of the femurs from wild-

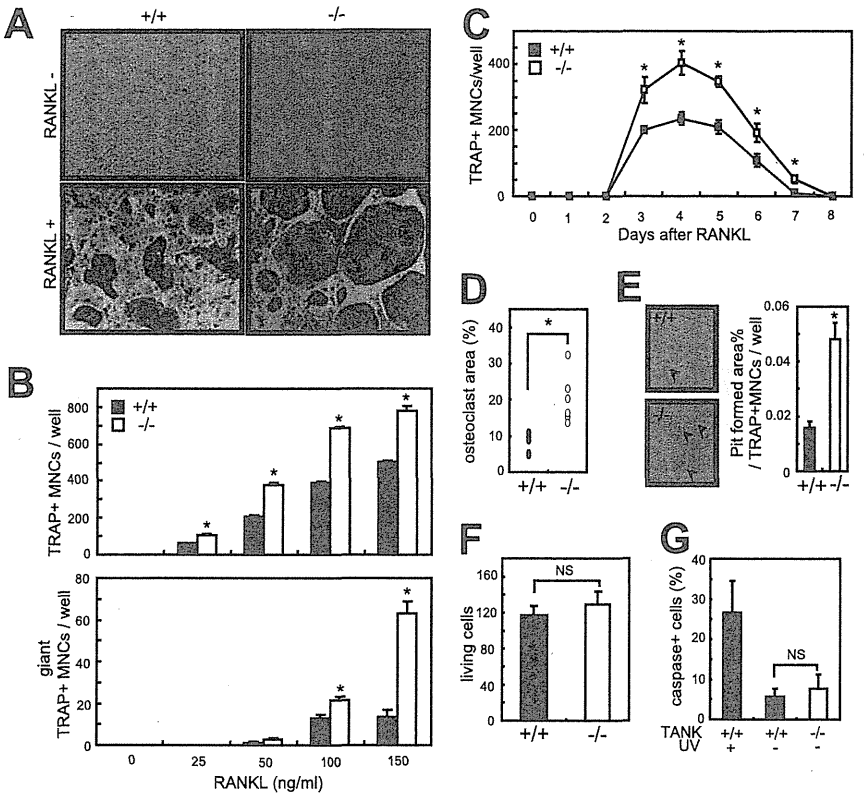

FIGURE 2. **Osteoclast differentiation is increased in *Tank*$^{-/-}$ MDMs.** *A*, MDMs from wild-type and *Tank*$^{-/-}$ mice were cultured in the presence of 100 ng/ml RANKL. After 3 days, TRAP staining was performed. *B*, numbers of TRAP-positive multinucleated (>3 nuclei/cell identified in a ×10 field) cells and giant TRAP-positive multinucleated (>20 nuclei/cell) cells were counted. Error bars: S.E. ($n = 3$). *, $p < 0.05$ *versus* wild-type. *C*, sequential TRAP staining to count the numbers of osteoclasts from wild-type and *Tank*$^{-/-}$ MDMs (RANKL, 50 ng/ml). Error bars: S.E. ($n = 3$). *, $p < 0.05$ *versus* 0 h. *D*, osteoclast areas (percentages of TRAP-positive multinucleated cells relative to the total area) were measured using ImageJ (RANKL, 100 ng/ml) and normalized by osteoclast number. Error bars: S.E. ($n = 6$). *, $p < 0.05$. *E*, formation of resorption pits by osteoclasts induced from wild-type or *Tank*$^{-/-}$ mice (RANKL, 50 ng/ml). Error bars: S.E. ($n = 3$). *, $p < 0.05$. *F*, MDMs were stained with trypan blue, and the numbers of viable cells were determined under a light microscope. *G*, apoptosis of wild-type and *Tank*$^{-/-}$ MDMs. Caspases were stained using a Poly Caspase Assay Kit, and the numbers of caspase-positive cells were counted under a fluorescence microscope. The data shown are representative of three (*A*, *B*, *D*, *F*, and *G*) and two (*C* and *E*) independent experiments.

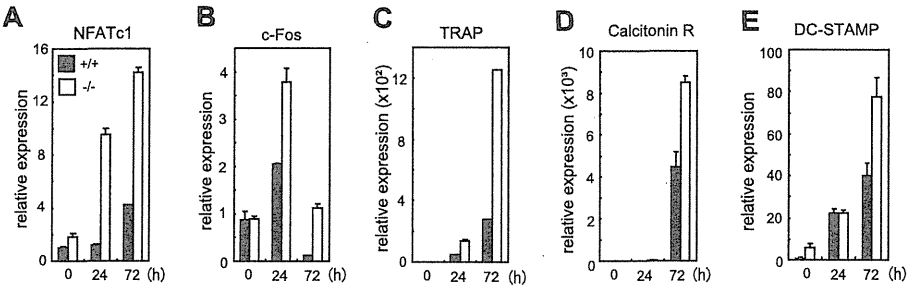

FIGURE 3. **TANK negatively regulates the expressions of osteoclastogenic genes.** *A–E*, quantitative PCR analyses of osteoclastogenic marker genes in wild-type and *Tank*$^{-/-}$ cells cultured with M-CSF alone (0 h) or 50 ng/ml RANKL plus M-CSF (24 and 72 h). Error bars: S.D. ($n = 2$). *Filled bars*: wild-type; *open bars*: knock-out. The data shown are representative of three independent experiments.

type and *Tank*$^{-/-}$ mice. As expected, the maximum load and stiffness showed slight, but not significant, increases in the femurs from *Tank*$^{-/-}$ mice. Furthermore, the femurs from *Tank*$^{-/-}$ mice showed 2-fold increases in the post-yield deflection and work to failure compared with the femurs from wild-type mice (Fig. 5*D*). These findings indicate that the femurs of *Tank*$^{-/-}$ mice are more ductile than those of wild-type mice. Next, we cut the proximal one-third of the right shaft of femurs and cross sections were made. We performed the histomorphometric analysis and detected dramatically increased eroded surface/bone surface in endosteum (Fig. 5*E*). Furthermore, bone forming rate in periosteum was increased, but not significant (Fig. 5*F*). Additionally, endosteum surface was comparable (this means bone marrow cavity perimeter was comparable) but cortical thickness was significantly increased in TANK-deficient mice (supplemental Fig. S2).

In contrast to the increased BMD and cortical area in the proximal to mid-shaft portion, the distal portion of the femurs from *Tank*$^{-/-}$ mice exhibited severe trabecular bone loss, as observed in three-dimensional images (Fig. 5*F*). Morphometric

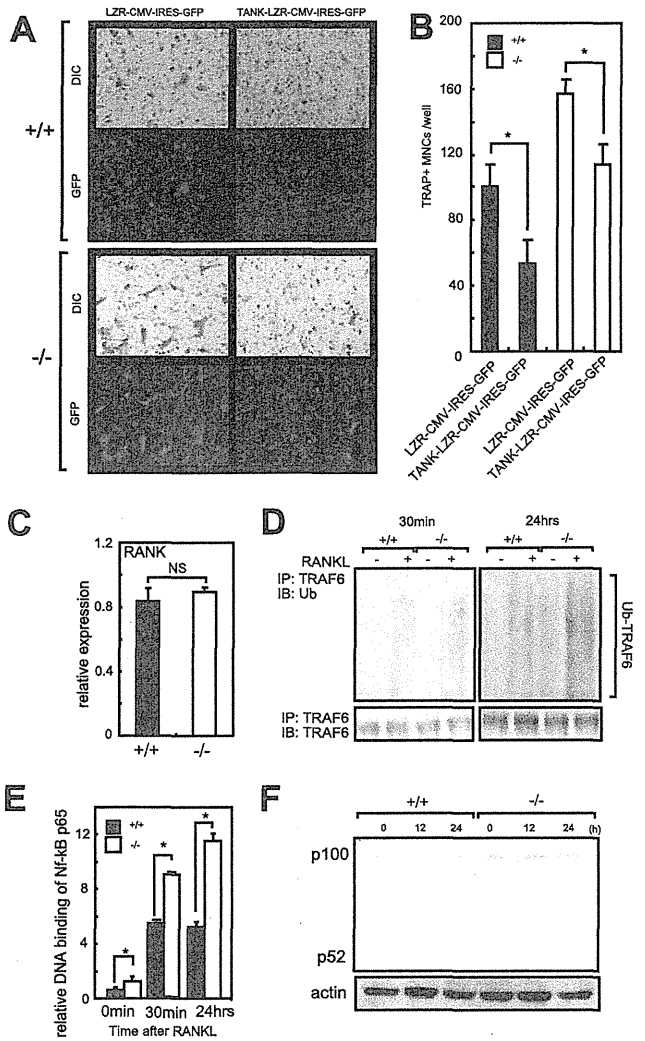

FIGURE 4. **TANK negatively regulates TRAF6 ubiquitination and NF-κB p65 activation, and its overexpression attenuates osteoclast differentiation.** *A*, MDMs from wild-type *Tank*$^{-/-}$ mice were retrovirally transfected with empty vector (LZR-CMV-IRES-GFP) or vector expressing TANK (TANK-LZR-CMV-IRES-GFP). After 3 days of culture with 25 ng/ml M-CSF plus 50 ng/ml RANKL, GFP-positive cells were identified by fluorescence microscopy (*GFP*) and the cells were stained for TRAP (*DIC*). *C*, mRNA levels of RANK in MDMs were measured by quantitative PCR ($n = 3$). *D*, immunoblotting analysis of anti-TRAF6 antibody immunoprecipitates from MDMs stimulated with RANKL (350 ng/ml) for indicated times probed with an anti-Ub antibody. As a loading control, immunoblotting analysis of TRAF6 was performed (*bottom*). *E*, DNA binding activity of NF-κB p65 in response to RANKL was measured using a TransAM Transcription Factor Assay Kit. Error bars: S.E. ($n = 3$). *, $p < 0.05$. *F*, MDMs were treated with RANKL for the indicated time and analyzed by Western blotting using anti-p100/p52 antibodies. Actin was evaluated as a loading control. The data shown are representative of three independent experiments.

analyses of the distal femurs from *Tank*$^{-/-}$ mice revealed pronounced reductions in the trabecular bone volume per tissue volume and trabecular bone number (Fig. 5*G*). Analyses of the proximal tibias from *Tank*$^{-/-}$ mice also indicated a decrease in the trabecular bone number, but no significant decrease in the trabecular bone thickness, compared with wild-type mice (Fig. 5, *H* and *I*). Histomorphometric analyses revealed that the eroded surface per bone surface and bone formation rate of the proximal tibias from *Tank*$^{-/-}$ mice were significantly increased. Furthermore, comparable numbers of osteoclasts and osteoblasts were observed for wild-type and *Tank*$^{-/-}$ mice (Fig. 5*J*), suggesting enhancement of the osteoclast function in *Tank*$^{-/-}$ mice. Consistent with the increased bone eroded surface and bone formation, the serum levels of the bone resorption marker TRACP5, cross-linked C-Telopeptide of Type I collagen (CTX-I), and bone formation marker ALP were higher in *Tank*$^{-/-}$ mice than in wild-type mice (Fig. 5*K*). In contrast, serum RANKL and OPG levels were comparable (Fig. 5*L*). These findings suggest that *Tank*$^{-/-}$ mice exhibit increased cortical BMD in the proximal to mid-shaft femur, but severe trabecular bone loss in the distal femur and proximal tibia.

Increased Bone Nodule Formation in Tank$^{-/-}$ *Osteoblasts*—Because the increased osteoclastogenesis contradicted the increased BMD, we examined the function of calvarial osteoblasts from *Tank*$^{-/-}$ mice. The expression of TANK mRNA was up-regulated during *in vitro* osteoblast differentiation (Fig. 6*A*). During the differentiation, there were no significant differences in the cell numbers between wild-type and *Tank*$^{-/-}$ osteoblasts (Fig. 6*B*). Next, to analyze the bone nodule formation by osteoblasts, the cultured cells were stained with alizarin red. Interestingly, *Tank*$^{-/-}$ osteoblasts showed increased bone nodule formation (Fig. 6, *C* and *D*). The ALP activity, as a phenotypic marker of osteoblasts, was also elevated in *Tank*$^{-/-}$ osteoblasts (Fig. 6, *E* and *F*). To search for the osteoblastic factor responsible for the osteoclastogenesis, we examined the expression levels of Runx2, RANKL, and OPG in osteoblasts, and found that the expression levels of Runx2 and RANKL, but not OPG, were significantly up-regulated in *Tank*$^{-/-}$ cells (Fig. 6*G*). Osteoclast-osteoblast coculture assays indicated that the increased RANKL expression in *Tank*$^{-/-}$ osteoblasts potentiate osteoclastogenesis *in vitro* (Fig. 6*H*). To reveal the mechanisms of increased osteoblast functions in *Tank*$^{-/-}$ mice, we checked the activation of DNA binding activity of NF-κB p65 in osteoblasts, and observed the 2-fold increase of NF-κB activation in TANK-deficient osteoblast compared with wild-type control (Fig. 6*I*). It has been known that increased NF-κB activation leads to induce IL-6-type cytokines such as IL-6, IL-11 and OncostatinM. Importantly, previous reports have established that IL-6-type cytokines play a pivotal role in bone metabolism (22). Thus, we next checked the expression levels of IL-6-type cytokines in TANK-deficient osteoblasts (Fig. 6*J*). Intriguingly, mRNA levels of IL-6 and IL-11 (especially IL-11) are significantly increased in TANK-deficient osteoblasts compared with wild-type controls (Fig. 6*J*). When we cultured osteoblasts with NF-κB inhibitor BAY117085, IL-11 mRNA level was significantly inhibited in TANK-deficient osteoblast (Fig. 6*K*). IL-6-type cytokines are potent stimulators of the development of osteoblastogenesis. Thus, our findings above prompted us to explore the effect of IL-6 and IL-11 neutralizing antibodies on *in vitro* bone nodule formation in TANK-deficient osteoblasts (Fig. 6, *L* and *M*). IL-6 neutralizing antibody had no effect to bone nodule formation in TANK-deficient osteoblasts (Fig. 6*L*). In contrast, IL-11 neutralizing antibody significantly suppressed the bone nodule formation in TANK-deficient osteobalsts to the same level as wild-type controls (Fig. 6, *L* and *M*). These findings suggest that increased IL-11 expression is at least partially attributed to increased NF-κB activation

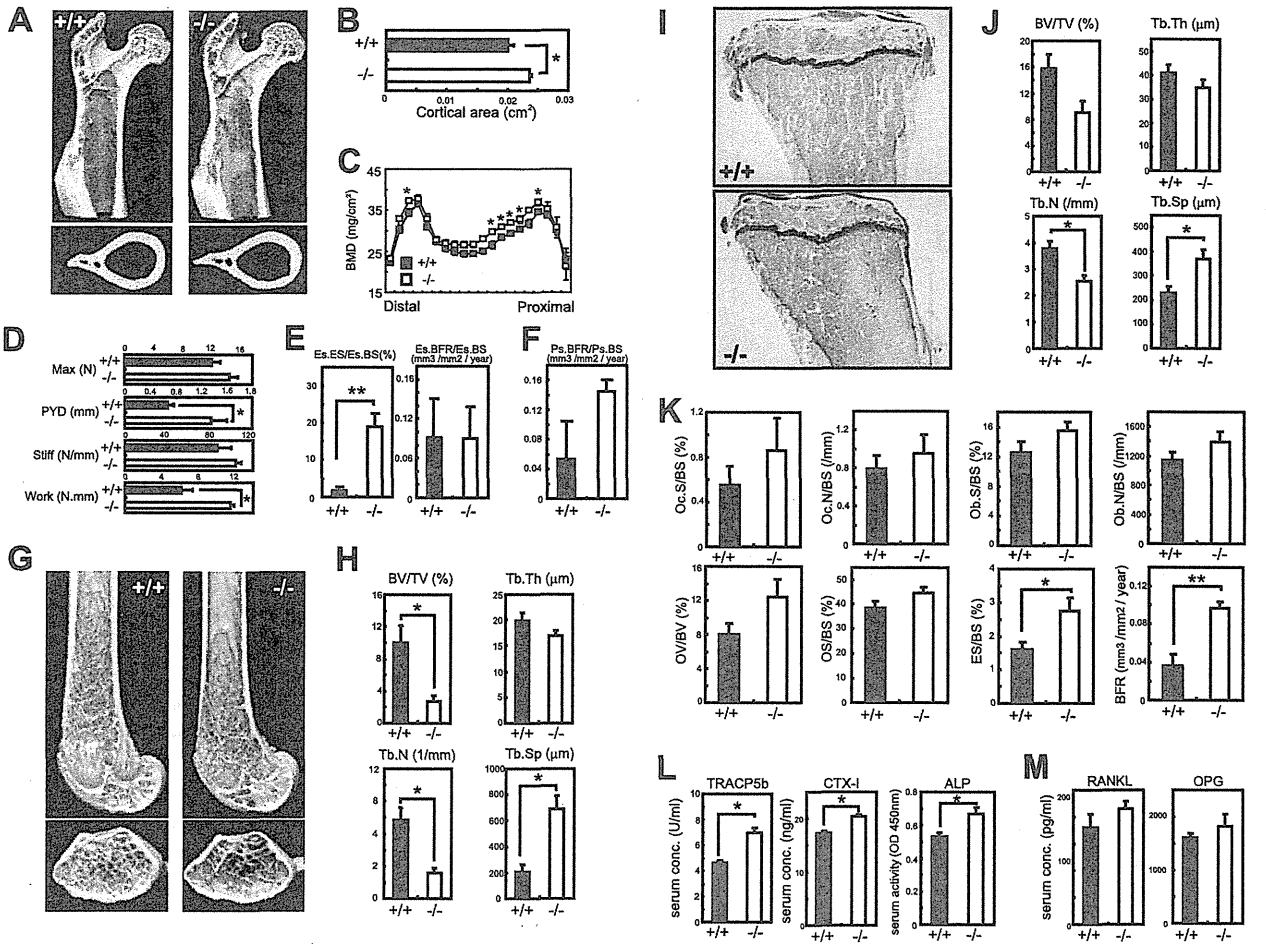

FIGURE 5. **Tank$^{-/-}$ mice exhibit severe trabecular bone loss, but increased cortical BMD.** *A*, representative images of proximal femurs from 10-week-old wild-type and *Tank*$^{-/-}$ mice (*upper*: longitudinal view; *lower*: axial view of the region of the third trochanter). *B*, cortical areas of the mid-shaft section in the femurs. Error bars: S.E. ($n = 3$). *, $p < 0.05$. *C*, BMDs in 20 longitudinal divisions of the femurs. Error bars: S.E. ($n = 3$). *, $p < 0.05$. *D*, mechanical properties of the femur shafts were measured by a three-point bending test. The whole bone mechanical properties of maximum load (*N*), stiffness (*N/mm*), post-yield deflection (*mm*), and work to failure (*N.mm*) were measured. Error bars: S.E. ($n = 3$). *, $p < 0.05$. *E*, bone histomorphometric analyses of the endosteum portion of cross section from proximal one-third of femur. *Es.ES/Es.BS*, endosteum eroded surface per endosteum bone surface; *Es.BFR/Es.BS*, endosteum bone formation rate per endosteum bone surface. Error bars: S.E. ($n = 3$). *, $p < 0.05$. *F*, bone histomorphometric analyses of the periosteum portion of cross section from proximal one-third of femur. *Ps.BFR/Ps.BS*, periosteum bone formation rate per periosteum bone surface. Error bars: S.E. ($n = 3$). *, $p < 0.05$. *G*, representative images of distal femurs from 10-week-old wild-type and *Tank*$^{-/-}$ mice (*upper*: longitudinal view; *lower*: axial view of the metaphyseal region). *H*, bone morphometric analyses of distal femurs from wild-type and *Tank*$^{-/-}$ mice using μCT. Error bars: S.E. ($n = 4$). *, $p < 0.05$. *I*, representative images of the metaphyseal portion of tibias from wild-type and *Tank*$^{-/-}$ mice (Villanueva bone staining). *J* and *K*, bone histomorphometric analyses of the metaphyseal portion of tibias from wild-type and *Tank*$^{-/-}$ mice. Error bars: S.E. ($n = 4$). *, $p < 0.05$, **, $p < 0.01$. *L*, serum concentrations of TRACP5b, CTX-I and ALP in wild-type and *Tank*$^{-/-}$ mice. Error bars: S.E. ($n = 4$) *, $p < 0.05$. *M*, serum concentrations of RANKL and OPG. Error bars: S.E. ($n = 4$) *, $p < 0.05$. *BV/TV*, bone volume per tissue volume; *Tb.Th*, trabecular bone thickness; *Tb.N*, trabecular bone number; *Tb.Sp*, trabecular bone spacing; *Oc.S/BS*, osteoclast surface per bone surface; *Oc.N/BS*, osteoclast number per bone surface; *Ob.S/BS*, osteoblast surface per bone surface; *Ob.N/BS*, osteoblast number per bone surface; *OV/BV*, osteoid volume per bone volume; *OS/BS*, osteoid surface per bone surface; *ES/BS*, eroded surface per bone surface; *BFR*, bone formation rate.

and such enhanced IL-11 production promotes the bone formation in TANK-deficient osteoblasts. Collectively, these findings suggest that TANK is a negative regulator of osteoblast bone formation and IL-11 is a critical target of TANK in osteoblasts.

Trabecular Bone Loss in Tank$^{-/-}$ Mice Is Dependent on Hematopoietic Cells—To examine whether the severe trabecular bone loss in *Tank*$^{-/-}$ mice could be explained by TANK deficiency in osteoclasts, we generated bone marrow chimeric mice. TANK expression in splenocytes and protein in bone marrow cells from wild-type mice engrafted with bone marrow from *Tank*$^{-/-}$ mice (−/− → WT mice) was scarcely detected (Fig. 7, *A* and *D*). CD11b+RANK+ osteoclast precursor populations in splenocytes were comparable between −/− → WT and +/+ → WT mice (supplemental Fig. S3). MDMs from −/− → WT mice efficiently differentiated into osteoclasts *in vitro* (Fig. 7*B*) rather than MDMs from wild-type mice engrafted with bone marrow from wild-type mice (+/+ → WT mice). Consistent with the *Tank*$^{-/-}$ mice, −/− → WT mice exhibited severe trabecular bone loss in their femurs and tibias compared with +/+ → WT mice (Fig. 7, *C* and *F*). Morphometric analyses of the femurs from −/− → WT mice revealed severe reductions in the trabecular bone volume per tissue volume and trabecular bone number (Fig. 7*E*). Analyses of the proximal tibias from −/− → WT mice also indicated decreases in the trabecular bone volume per tissue volume and trabecular

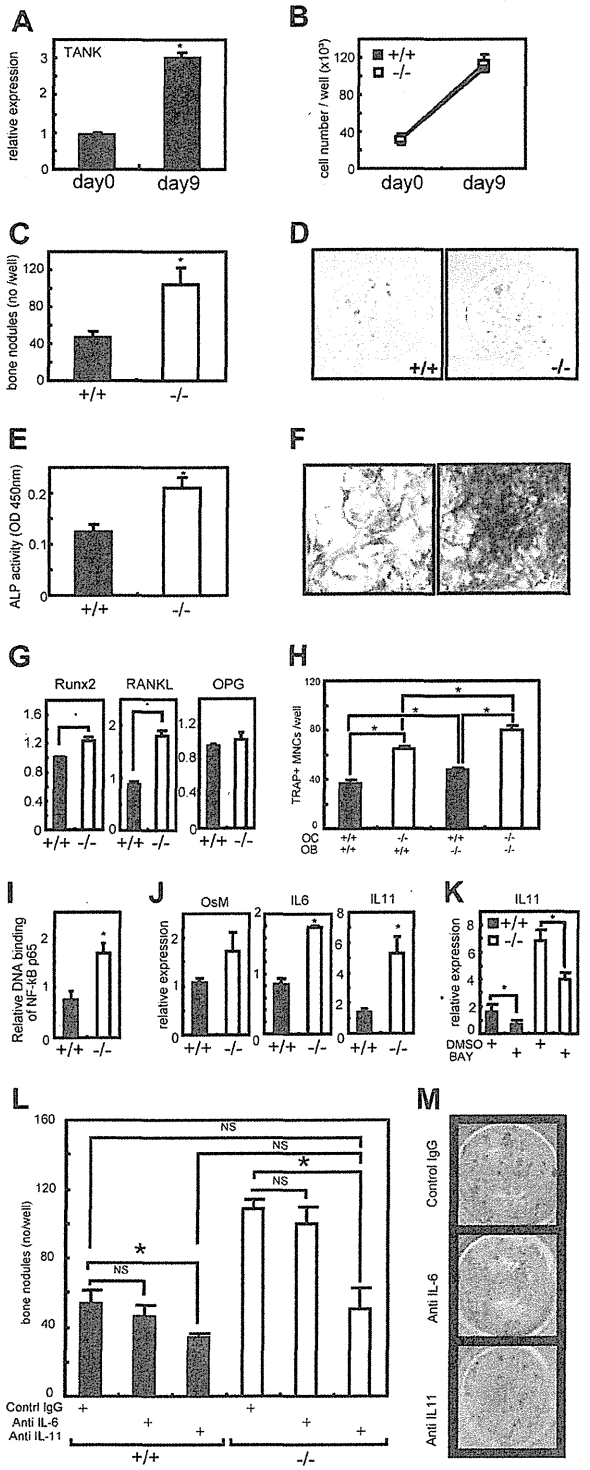

FIGURE 6. **Increased bone formation by $Tank^{-/-}$ calvarial osteoblasts.** *A*, calvariae from wild-type mice were treated with an osteoblast-inducing reagent for 9 days. The mRNA levels of TANK were measured by quantitative PCR. Error bars: S.E. ($n = 3$). *, $p < 0.05$ *versus* d 0. *B*, numbers of osteoblasts in culture. *C*, osteoblasts (after a 9-day culture of calvariae) were stained with a calcified nodule staining kit, and the numbers of bone nodules were counted. Error bars: S.E. ($n = 3$). *, $p < 0.05$ *versus* wild-type. *D*, representative images of calcified nodules in *C*. *E*, ALP activities in homogenates of the osteoblasts. Error bars: S.E. ($n = 3$). *, $p < 0.05$ *versus* wild-type. *F*, representative images of ALP staining in osteoblasts. *G*, mRNA levels of Runx2, RANKL, and OPG were measured by quantitative PCR. Error bars: S.E. ($n = 3$). *, $p < 0.05$, *versus* wild-type. *H*, bone marrow cells (*OC*) and calvariae (*OB*) were cocultured in the presence of $1\alpha,25(OH)_2D_3$ for 10 days. The numbers of TRAP-positive multinucleated cells were counted. Error bars: S.E. ($n = 3$). *, $p < 0.05$. *I*, DNA binding activity of NF-κB p65 in osteoblasts (after a 9-day culture of calvariae) was measured using a TransAM Transcription Factor Assay Kit. Error bars: S.E. ($n = 3$). *, $p < 0.05$. *J*, quantitative PCR analyses OncostatinM (OsM), IL-6, and IL-11 in osteobalsts. Error bars: S.E. ($n = 3$). *, $p < 0.05$. *K*, 5 mM NF-κB inhibitor BAY117085 was added to the osteoblast culture for 24 h and IL-11 mRNA level was quantified. Error bars: S.E. ($n = 3$). *, $p < 0.05$. *L*, calvarial osteoblasts were cultured with neutralizing antibodies of IL-6 and IL-11. After a 9-day culture, cells were stained with a calcified nodule staining kit, and the numbers of bone nodules were counted. Error bars: S.E. ($n = 3$). *, $p < 0.05$. *M*, representative images of bone nodules formed by $Tank^{-/-}$ calvarial osteoblasts in *L*.

bone number compared with +/+ → WT mice (Fig. 7*G*). The osteoblast numbers were comparable between both types of chimeric mice, although the number was slightly, but not significantly, increased in the proximal end of the tibias from −/− → WT mice (Fig. 7*H*). Additionally, cortical thickness was decreased (Fig. 7*I*) and eroded surface/bone surface was drastically increased in endosteum from −/− → WT mice (Fig. 7*J*). Further, the serum levels of the bone resorption marker TRACP5b were higher in −/− → WT mice than in +/+ → WT mice but ALP levels were comparable (Fig. 7*K*). The trabecular bone structural analogy between $Tank^{-/-}$ mice and −/− → WT mice demonstrates that the trabecular bone loss in $Tank^{-/-}$ mice is caused by hematopoietic cells including osteoclasts.

DISCUSSION

In the present study, we have shown that TANK is a novel regulator of osteoclastogenesis and bone formation. TANK deficiency caused significant trabecular bone loss in the femur and tibia. *In vitro* osteoclastogenesis of $Tank^{-/-}$ bone marrow cells was enhanced because of increased RANK signaling. Consistently, *in vivo* bone erosion by osteoclasts was significantly increased, which may explain the trabecular bone loss phenotype under TANK deficiency. However, we also found that lack of TANK led to increased bone formation and BMD in the proximal cortical portion of the femur. Bone nodule formation by *in vitro* cultured calvarial osteoblasts from TANK-deficient mice was also up-regulated. Collectively, these findings suggest that TANK negatively controls the functions of bone formation and erosion.

We have shown that osteoclasts lacking TANK exhibit increased bone-resorbing function both *in vitro* and *in vivo*. Expression of TANK was significantly increased during RANKL-induced osteoclastogenesis, while overexpression of TANK led to suppressed osteoclastogenesis. These observations support the idea that TANK acts as a negative regulator of osteoclastogenesis. Our previous report clarified that macrophages and B cells from $Tank^{-/-}$ mice exhibit enhanced canonical NF-κB and AP-1 activation in response to stimulation of TLRs and BCR (19). The RANKL-induced NF-κB pathways include canonical and non-canonical pathways involving the NF-κB precursor proteins p105 and p100, respectively. Previous reports have suggested that mice lacking both NF-κB subunits p50 and p52 develop osteopetrosis, accompanied by a reduction in osteoclastogenesis (4) (8). In these mice, both the canonical and non-canonical NF-κB pathways are inhibited. Alymphoplasia mice, in which processing of p100 to p52 does

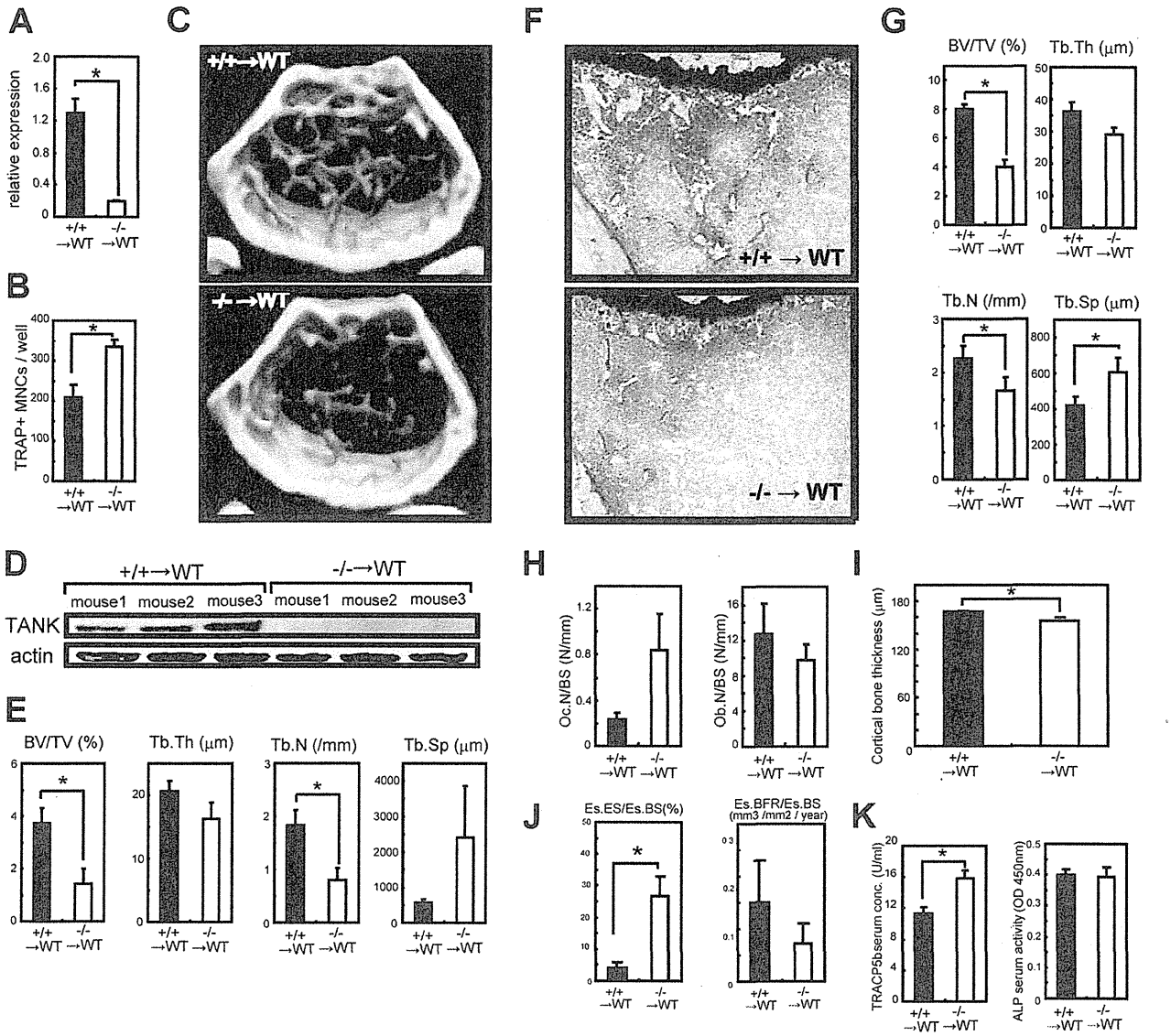

FIGURE 7. **Wild-type mice engrafted with *Tank*$^{-/-}$ bone marrow exhibit severe bone loss.** *A*, expression levels of TANK in splenocytes from wild-type mice engrafted with wild-type marrow (+/+ → WT) and *Tank*$^{-/-}$ marrow (−/− → WT) specimens were measured by quantitative PCR. *B*, MDMs from +/+ → WT and −/− → WT specimens were treated with 50 ng/ml RANKL for 3 days and the numbers of osteoclasts were counted. *C*, representative images of distal femurs from +/+ → WT and −/− → WT specimens. *D*, TANK protein expression levels in bone marrow cells from +/+ → WT and −/− → WT mice. *E*, bone morphometric analyses of distal femurs from +/+ → WT and −/− → WT specimens using μCT. *F*, representative photographs of the metaphyseal portion of tibias from +/+ → WT and −/− → WT specimens (Villanueva bone staining). *G* and *H*, bone histomorphometric analyses of tibias from +/+ → WT and −/− → WT specimens. *I*, cortical bone thickness in the portion of cross section from proximal one-third of femur. Error bars: S.E. ($n = 3$). *, $p < 0.05$. *J*, bone histomorphometric analyses of the endosteum portion of cross section from proximal one-third of femur. Error bars: S.E. ($n = 3$). *, $p < 0.05$. *K*, serum concentrations of TRACP5b and ALP in +/+ → WT and −/− → WT mice. Error bars: S.E. ($n = 3$). *, $p < 0.05$. *BV/TV*, bone volume per tissue volume; *Tb.Th*, trabecular bone thickness; *Tb.N*, trabecular bone number; *Tb.Sp*, trabecular bone spacing; *Oc.N/BS*, osteoclast number per bone surface; *Ob.N/BS*, osteoblast number per bone surface. *Es.ES/Es.BS*, endosteum eroded surface per endosteum bone surface; *Es.BFR/Es.BS*, endosteum bone formation rate per endosteum bone surface.

not occur owing to an inactive form of NIK (23), show mild osteopetrosis caused by significantly reduced osteoclastogenesis (24). These reports strongly suggest that both the canonical and non-canonical NF-κB pathways are important for efficient osteoclastogenesis. NFATc1 is a master regulator of osteoclastogenesis, and we found that the level of NFATc1 expression during osteoclastogenesis was increased in *Tank*$^{-/-}$ cells. Since NF-κB has been implicated in the induction of NFATc1 in RANKL signaling, we examined whether the loss of TANK also promoted NF-κB activation in response to RANKL, and found that canonical NF-κB pathway activation was significantly elevated in *Tank*$^{-/-}$ macrophages. In contrast, the non-canonical NF-κB pathway was not altered, suggesting that TANK negatively regulates canonical NF-κB pathway activation in response to RANKL, synonymous with TLR and BCR stimulation. These findings suggest that augmentation of canonical NF-κB activation alone is sufficient for controlling osteoclastogenesis. Several molecules have been characterized to play inhibitory roles in osteoclastogenesis. IRAK-M, a negative regulator of TLR/IL-1R signaling, acts as an inhibitor of osteoclast

differentiation and activation, probably by suppressing IL-1R signaling in inflammation (25). Another example is Src homology 2-containing inositol-5-phosphatase (SHIP), which limits osteoclast precursor survival and differentiation by suppressing PI3-kinase (26). On the other hand, the regulation of RANKL-mediated signaling is less well characterized, except for CYLD. This molecule is a deubiquitinating enzyme induced by RANKL that suppresses RANK signaling by inhibiting TRAF6 ubiquitination (27). In this study, we found that TANK specifically inhibited RANKL-induced osteoclastogenesis under physiological conditions, synonymous with CYLD, and suggest a model whereby negative feedback regulation of RANKL signaling by TANK contributes to proper osteoclast differentiation. Information on the relationship between TANK and CYLD would be important for the future study. Although we observed enhanced TRAF6 ubiquitination in *TANK*$^{-/-}$ cells in response to RANKL stimulation, the effect of TANK deficiency was relatively modest. Thus, it is possible that a mechanism other than TRAF6 polyubiquitination also contribute to TANK-mediated control of osteoclastogenesis. Further detailed studies are needed to explore the role of TANK in osteoclasts.

Abnormal bone turnover is observed in several human diseases. Rheumatoid arthritis is a major high-bone turnover osteoporotic disease (28). Paget disease is also characterized by accelerated bone resorption by IL-6-producing giant osteoclasts and enhanced bone formation by osteoblasts, resulting in increased BMD and bone fragility (29). Schnitzler's syndrome is another high-bone turnover disorder, and is characterized by osteosclerosis, chronic urticaria, lymphadenopathy, IgM gammopathy, and joint pain (30, 31). Our previous report indicated that lymphadenopathy and increased basal serum concentrations of IgM were the major features in *Tank*$^{-/-}$ mice (19). Since TANK deficiency closely resembles some of the traits of the human high-bone turnover diseases described above, the involvement of TANK in these disorders must be clarified in the future.

As observed in the *in vivo* bone analyses, TANK suppresses both osteoclasts and osteoblasts. Bone formation and degradation are often manipulated simultaneously in the same direction, which is termed coupling (32). Such coupling events are crucial for the maintenance of bone quality. Understanding of coupling is important, but its molecular mechanisms are largely unknown. As TANK has a dual suppressive effect on both cell types, it may play a role, at least in part, in supporting the speed of such coupling. Intriguingly, *Tank*$^{-/-}$ mice seem to suffer from osteosclerosis and osteoporosis in the cortical and trabecular bone areas, respectively. In other words, *Tank*$^{-/-}$ bone has an abnormal morphology. Our detailed cellular studies in both osteoclasts and osteoblasts *in vitro*, *Tank*$^{-/-}$ mice have intrinsic abnormalities in the functions of both cell types. It is still unclear how TANK inhibits bone formation in osteoblasts. The ALP activity and expression level of Runx2, an essential transcription factor for the regulation of osteoblast differentiation (33), were slightly increased, suggesting that TANK may partially regulate osteoblast differentiation. Our data also indicated that increased IL-11 expression is at least partially attributed to increased NF-κB activation and such enhanced IL-11 production promotes the bone formation in TANK-deficient osteoblasts. Further detailed studies are needed to explore the role of TANK in osteoblast function, but our observations suggest for the first time that IL-11 is a critical target of TANK in osteoblasts.

Finally, considering the *Tank*$^{-/-}$ bone phenotype and suppressive functions of TANK toward both osteoclasts and osteoblasts, modulation of TANK will potentially result in distinct prophylactic effects, depending on the trabecular and cortical portions. Further, generation of methods for the inhibition and stimulation of TANK in osteoblasts and osteoclasts, respectively, may be a reasonable strategy to manipulate bone-destructive diseases.

Acknowledgments—We thank J. Kikuta, M. Ishii, H. Iwasaki, T. Satoh, and D. Ori for technical advice, E. Kamada and M. Kageyama for secretarial assistance, Y. Fujiwara, M. Kumagai, and N. Umano for technical assistance, and T. Imamura and S. Tartey for participating in fruitful discussions.

REFERENCES

1. Karsenty, G., and Wagner, E. F. (2002) Reaching a genetic and molecular understanding of skeletal development. *Dev. Cell* **2,** 389–406
2. Takayanagi, H., Kim, S., Koga, T., Nishina, H., Isshiki, M., Yoshida, H., Saiura, A., Isobe, M., Yokochi, T., Inoue, J., Wagner, E. F., Mak, T. W., Kodama, T., and Taniguchi, T. (2002) Induction and activation of the transcription factor NFATc1 (NFAT2) integrate RANKL signaling in terminal differentiation of osteoclasts. *Dev. Cell* **3,** 889–901
3. Grigoriadis, A. E., Wang, Z. Q., Cecchini, M. G., Hofstetter, W., Felix, R., Fleisch, H. A., and Wagner, E. F. (1994) c-Fos: a key regulator of osteoclast-macrophage lineage determination and bone remodeling. *Science* **266,** 443–448
4. Franzoso, G., Carlson, L., Xing, L., Poljak, L., Shores, E. W., Brown, K. D., Leonardi, A., Tran, T., Boyce, B. F., and Siebenlist, U. (1997) Requirement for NF-κB in osteoclast and B-cell development. *Genes Dev.* **11,** 3482–3496
5. Yamashita, T., Yao, Z., Li, F., Zhang, Q., Badell, I. R., Schwarz, E. M., Takeshita, S., Wagner, E. F., Noda, M., Matsuo, K., Xing, L., and Boyce, B. F. (2007) NF-κB p50 and p52 regulate receptor activator of NF-κB ligand (RANKL) and tumor necrosis factor-induced osteoclast precursor differentiation by activating c-Fos and NFATc1. *J. Biol. Chem.* **282,** 18245–18253
6. Yagi, M., Miyamoto, T., Sawatani, Y., Iwamoto, K., Hosogane, N., Fujita, N., Morita, K., Ninomiya, K., Suzuki, T., Miyamoto, K., Oike, Y., Takeya, M., Toyama, Y., and Suda, T. (2005) DC-STAMP is essential for cell-cell fusion in osteoclasts and foreign body giant cells. *J. Exp. Med.* **202,** 345–351
7. Yagi, M., Ninomiya, K., Fujita, N., Suzuki, T., Iwasaki, R., Morita, K., Hosogane, N., Matsuo, K., Toyama, Y., Suda, T., and Miyamoto, T. (2007) Induction of DC-STAMP by alternative activation and downstream signaling mechanisms. *J. Bone Miner Res.* **22,** 992–1001
8. Iotsova, V., Caamaño, J., Loy, J., Yang, Y., Lewin, A., and Bravo, R. (1997) Osteopetrosis in mice lacking NF-κB1 and NF-κB2. *Nat. Med.* **3,** 1285–1289
9. Leibbrandt, A., and Penninger, J. M. (2008) RANK/RANKL: regulators of immune responses and bone physiology. *Ann. N.Y. Acad. Sci.* **1143,** 123–150
10. Naito, A., Azuma, S., Tanaka, S., Miyazaki, T., Takaki, S., Takatsu, K., Nakao, K., Nakamura, K., Katsuki, M., Yamamoto, T., and Inoue, J. (1999) Severe osteopetrosis, defective interleukin-1 signaling and lymph node organogenesis in TRAF6-deficient mice. *Genes Cells* **4,** 353–362
11. Lomaga, M. A., Yeh, W. C., Sarosi, I., Duncan, G. S., Furlonger, C., Ho, A., Morony, S., Capparelli, C., Van, G., Kaufman, S., van der Heiden, A., Itie, A., Wakeham, A., Khoo, W., Sasaki, T., Cao, Z., Penninger, J. M., Paige, C. J., Lacey, D. L., Dunstan, C. R., Boyle, W. J., Goeddel, D. V., and Mak,

T. W. (1999) TRAF6 deficiency results in osteopetrosis and defective interleukin-1, CD40, and LPS signaling. *Genes Dev.* **13,** 1015–1024
12. Kobayashi, T., Walsh, P. T., Walsh, M. C., Speirs, K. M., Chiffoleau, E., King, C. G., Hancock, W. W., Caamano, J. H., Hunter, C. A., Scott, P., Turka, L. A., and Choi, Y. (2003) TRAF6 is a critical factor for dendritic cell maturation and development. *Immunity* **19,** 353–363
13. Akira, S., Uematsu, S., and Takeuchi, O. (2006) Pathogen recognition and innate immunity. *Cell* **124,** 783–801
14. Takeuchi, O., and Akira, S. (2010) *Cell* **140,** 805–820
15. Cheng, G., and Baltimore, D. (1996) TANK, a co-inducer with TRAF2 of TNF- and CD 40L-mediated NF-kappaB activation. *Genes Dev.* **10,** 963–973
16. Rothe, M., Xiong, J., Shu, H. B., Williamson, K., Goddard, A., and Goeddel, D. V. (1996) I-TRAF is a novel TRAF-interacting protein that regulates TRAF-mediated signal transduction. *Proc. Natl. Acad. Sci. U.S.A.* **93,** 8241–8246
17. Chin, A. I., Shu, J., Shan Shi, C., Yao, Z., Kehrl, J. H., and Cheng, G. (1999) TANK potentiates tumor necrosis factor receptor-associated factor-mediated c-Jun N-terminal kinase/stress-activated protein kinase activation through the germinal center kinase pathway. *Mol. Cell Biol.* **19,** 6665–6672
18. Pomerantz, J. L., and Baltimore, D. (1999) NF-κB activation by a signaling complex containing TRAF2, TANK, and TBK1, a novel IKK-related kinase. *EMBO J.* **18,** 6694–6704
19. Kawagoe, T., Takeuchi, O., Takabatake, Y., Kato, H., Isaka, Y., Tsujimura, T., and Akira, S. (2009) TANK is a negative regulator of Toll-like receptor signaling and is critical for the prevention of autoimmune nephritis. *Nat. Immunol.* **10,** 965–972
20. Guo, B., and Cheng, G. (2007) Modulation of the interferon antiviral response by the TBK1/IKKi adaptor protein TANK. *J. Biol. Chem.* **282,** 11817–11826
21. Satoh, T., Kato, H., Kumagai, Y., Yoneyama, M., Sato, S., Matsushita, K., Tsujimura, T., Fujita, T., Akira, S., and Takeuchi, O. (2010) *Proc. Natl. Acad. Sci. U.S.A.* **107,** 1512–1517
22. Taguchi, Y., Yamamoto, M., Yamate, T., Lin, S. C., Mocharla, H., DeTogni, P., Nakayama, N., Boyce, B. F., Abe, E., and Manolagas, S. C. (1998) Interleukin-6-type cytokines stimulate mesenchymal progenitor differentiation toward the osteoblastic lineage. *Proc. Assoc. Am. Physicians* **110,** 559–574
23. Shinkura, R., Kitada, K., Matsuda, F., Tashiro, K., Ikuta, K., Suzuki, M., Kogishi, K., Serikawa, T., and Honjo, T. (1999) Alymphoplasia is caused by a point mutation in the mouse gene encoding Nf-κB-inducing kinase. *Nat. Genet.* **22,** 74–77
24. Maruyama, T., Fukushima, H., Nakao, K., Shin, M., Yasuda, H., Weih, F., Doi, T., Aoki, K., Alles, N., Ohya, K., Hosokawa, R., and Jimi, E. (2010) *J. Bone Miner Res.* **25,** 1058–1067
25. Li, H., Cuartas, E., Cui, W., Choi, Y., Crawford, T. D., Ke, H. Z., Kobayashi, K. S., Flavell, R. A., and Vignery, A. (2005) IL-1 receptor-associated kinase M is a central regulator of osteoclast differentiation and activation. *J. Exp. Med.* **201,** 1169–1177
26. Takeshita, S., Namba, N., Zhao, J. J., Jiang, Y., Genant, H. K., Silva, M. J., Brodt, M. D., Helgason, C. D., Kalesnikoff, J., Rauh, M. J., Humphries, R. K., Krystal, G., Teitelbaum, S. L., and Ross, F. P. (2002) SHIP-deficient mice are severely osteoporotic due to increased numbers of hyper-resorptive osteoclasts. *Nat. Med.* **8,** 943–949
27. Jin, W., Chang, M., Paul, E. M., Babu, G., Lee, A. J., Reiley, W., Wright, A., Zhang, M., You, J., and Sun, S. C. (2008) Deubiquitinating enzyme CYLD negatively regulates RANK signaling and osteoclastogenesis in mice. *J. Clin. Invest.* **118,** 1858–1866
28. Harris, E. D., Jr. (1990) Rheumatoid arthritis. Pathophysiology and implications for therapy. *N. Engl. J. Med.* **322,** 1277–1289
29. Roodman, G. D., and Windle, J. J. (2005) Paget disease of bone. *J. Clin. Invest.* **115,** 200–208
30. de Koning, H. D., Bodar, E. J., van der Meer, J. W., Simon, A., and Schnitzler Syndrome Study, G. (2007) Schnitzler syndrome: beyond the case reports: review and follow-up of 94 patients with an emphasis on prognosis and treatment. *Semin. Arthritis Rheum.* **37,** 137–148
31. Almerigogna, F., Giudizi, M. G., Cappelli, F., and Romagnani, S. (2002) Schnitzler's syndrome: what's new? *J. Eur. Acad. Dermatol. Venereol* **16,** 214–219
32. Feng, X., and McDonald, J. M. (2011) *Annu. Rev. Pathol.* **6,** 121–145
33. Komori, T., Yagi, H., Nomura, S., Yamaguchi, A., Sasaki, K., Deguchi, K., Shimizu, Y., Bronson, R. T., Gao, Y. H., Inada, M., Sato, M., Okamoto, R., Kitamura, Y., Yoshiki, S., and Kishimoto, T. (1997) Targeted disruption of Cbfa1 results in a complete lack of bone formation owing to maturational arrest of osteoblasts. *Cell* **89,** 755–764

J Gastroenterol (2012) 47:169–178
DOI 10.1007/s00535-011-0466-y

ORIGINAL ARTICLE—LIVER, PANCREAS, AND BILIARY TRACT

Dynamics of regulatory T cells and plasmacytoid dendritic cells as immune markers for virological response in pegylated interferon-α and ribavirin therapy for chronic hepatitis C patients

Tatsuya Kanto · Michiyo Inoue · Tsugiko Oze · Masanori Miyazaki · Mitsuru Sakakibara · Naruyasu Kakita · Tokuhiro Matsubara · Koyo Higashitani · Hideki Hagiwara · Sadaharu Iio · Kazuhiro Katayama · Eiji Mita · Akinori Kasahara · Naoki Hiramatsu · Tetsuo Takehara · Norio Hayashi

Received: 4 July 2011 / Accepted: 3 August 2011 / Published online: 27 September 2011

Abstract
Background For the treatment of chronic hepatitis C, a combination of pegylated interferon-α (PEG-IFNα) and ribavirin has been widely used as a standard of care. Enhancement of immune response against hepatitis C virus (HCV) is known to be involved in the efficacy of the combination therapy. Our aim was to elucidate whether or not the frequency or function of blood cells is related to the outcome of the therapy.
Methods Sixty-seven chronic hepatitis C patients with high viral load of HCV genotype 1 infection who underwent 48 weeks of PEG-IFNα2b and ribavirin therapy were examined. During the treatment, frequencies of myeloid or plasmacytoid dendritic cells, Th1, Th2 cells, NK cells, and regulatory T cells were phenotypically determined.
Results Among the patients enrolled, 29 showed a sustained virological response (SVR), 18 a transient response (TR) and 17 no response (NR). The clinical and immunological markers were compared between the SVR and non-SVR patients, including TR and NR. Based on clinical, histological, immunological parameters, and cumulative dosage of PEG-IFNα2b and ribavirin, multivariate analyses revealed that higher platelet counts and higher regulatory T cell frequency at week 12 are indicative of SVR. Even in patients who attained complete early virological response at week 12, multivariate analyses disclosed that higher platelet counts and higher plasmacytoid dendritic cell frequency are indicative of SVR.
Conclusions In PEG-IFNα and ribavirin combination therapy for chronic hepatitis C patients, the increments of regulatory T cells and plasmacytoid dendritic cell frequency are independently related to favorable virological response to the therapy.

Keywords Early virological response · Plasmacytoid dendritic cells · Regulatory T cells

T. Kanto (✉) · M. Inoue · T. Oze · M. Miyazaki · M. Sakakibara · N. Kakita · T. Matsubara · K. Higashitani · N. Hiramatsu · T. Takehara · N. Hayashi
Department of Gastroenterology and Hepatology, Osaka University Graduate School of Medicine, 2-2 Yamada-oka, Suita, Osaka 565-0871, Japan
e-mail: kantot@gh.med.osaka-u.ac.jp

T. Kanto
Department of Dendritic Cell Biology and Clinical Applications, Osaka University Graduate School of Medicine, Suita, Japan

Present Address:
M. Sakakibara · K. Katayama
Center for Adult Diseases of Osaka, Osaka, Japan

H. Hagiwara · S. Iio
Higashiosaka City General Hospital, Higashi-Osaka, Japan

Present Address:
H. Hagiwara · N. Hayashi
Kansai Rosai Hospital, Amagasaki, Japan

K. Katayama
Osaka Kosei-Nenkin Hospital, Osaka, Japan

E. Mita
National Hospital Organization Osaka National Hospital, Osaka, Japan

A. Kasahara
Department of General Medicine, Osaka University Hospital, Osaka, Japan

Introduction

Hepatitis C virus (HCV) is one of the major causative agents of chronic liver diseases and hepatocellular

carcinoma (HCC) in the world [1, 2]. In order to prevent the development of HCV-induced liver diseases, eradication of HCV from infected patients may be required. For the treatment of chronic hepatitis C, a combination of pegylated interferon-α (PEG-IFNα) and ribavirin treatment has been used as a standard of care (SOC) [3, 4]. However, in patients with HCV genotype 1 and high viral load, approximately 50% of them are able to clear the virus by 48 weeks of SOC [5, 6]. In addition to HCV genotype and quantity, several demographic factors have been reported as therapeutic determinants in PEG-IFNα and ribavirin therapy, such as age, gender, ethnicity, and liver fibrosis [5, 6]. In addition, it is accepted that initial changes of serum HCV RNA titer from the beginning of the therapy, i.e., early virological response (EVR), correlate well with the clinical outcomes of the treated patients [5, 7]. It has been reported that the patients who fail to clear HCV at week 24 are not likely to attain SVR after 48 weeks of the therapy, suggesting that non-EVR can serve as a negative predictor of SVR [8]. Even in patients who attained EVR, 30% of them eventually relapse during the 48 weeks of therapy. Prolongation of the duration of PEG-IFNα and ribavirin therapy from 48 to 72 weeks is recommended to improve the SVR rate by decreasing relapsers [9]. Thus, identifying potential relapsers during therapy and providing additional weeks of treatment may be clinically important, because it can offer them a better chance of attaining SVR.

In chronic hepatitis C, multifaceted immune dysfunction may be implicated in the persistence of HCV including dendritic cells (DC), NK cells, and T cells [10, 11]. Some investigators have reported that the dynamics of immune cells throughout the therapy are involved in the efficacy of PEG-IFNα and ribavirin. In chronic HCV infection, the enhancement of HCV-specific Th1 response or DC function has been reported to be involved in therapeutic HCV eradication [12, 13]. We have previously demonstrated that plasmacytoid dendritic cell (PDC) frequency and DC function are involved in HCV eradication in patients who underwent 48 weeks of PEG-IFNα and ribavirin therapy [14]. These reports have supported the possibility that the enhancement of certain immune responses is a prerequisite for therapeutic HCV clearance. However, one of the limitations of these studies is that the conclusions were drawn from relatively small numbers of patients and evaluated by univariate analysis. Therefore, multivariate analyses are arguably required in order to validate the significance or independence of immune cell markers in the therapeutic efficacy.

In this study, we have extended our investigation to elucidate whether or not the dynamics of immune cells are involved in therapeutic outcomes. Consequently, the independent significance of regulatory T cell or plasmacytoid DC frequency is revisited in the efficacy of PEG-IFNα and ribavirin therapy for chronic hepatitis C patients.

Materials and methods

Subjects

Among chronic hepatitis C patients who had been followed at Osaka University Hospital, Osaka Kosei-nenkin Hospital, Higashi Osaka Municipal Hospital, and Osaka National Hospital, 67 patients who received PEG-IFNα2b and ribavirin combination therapy for 48 weeks were enrolled in the present study. The study was approved by the ethics committee of the Osaka University Graduate School of Medicine and all the hospitals listed above (approval no. 08156). Written informed consent was obtained from all patients. At enrollment, the patients were confirmed to be positive for both serum anti-HCV antibody (Ab) and HCV RNA, but were negative for hepatitis B virus and human immunodeficiency virus. All of them were infected with HCV genotype 1b with serum HCV RNA quantity of more than 100 kilo international units (KIU)/ml, as determined by methods described elsewhere [15]. All patients had shown persistent or fluctuating serum alanine aminotransferase (ALT) abnormalities at enrollment. The presence of other causes of liver disease, such as autoimmune, alcoholic, and metabolic disorders was excluded by laboratory and imaging analyses. A combination of biochemical markers and ultrasonography (US) or computed tomography scan analyses ruled out the presence of cirrhosis and tumors in the liver in all patients. Histological analyses of liver disease were performed with liver tissue obtained by US-guided biopsy. The activity and stage of the disease were assessed by two independent pathologists according to the METAVIR scoring system [16].

Treatment

All patients were treated with PEG-IFNα2b subcutaneously at a dose of 75 μg/week (body weight >40 and ≤60 kg), 105 μg/week (body weight >60 and ≤80 kg), or 135 μg/week (body weight >80 and ≤100 kg) and oral ribavirin at a dose of 600 mg/day (body weight >40 and ≤60 kg), 800 mg/day (body weight >60 and ≤80 kg), or 1000 mg/day (body weight >80 and ≤100 kg). Ribavirin was administered divided into two doses per day. All patients were treated for 48 weeks and followed for 24 weeks after the cessation of therapy.

Dose reduction of PEG-IFNα and ribavirin

Dose modification followed, as a rule, the manufacturer's drug information according to the intensity of the hematological adverse effects. The dose of PEG-IFNα2b was reduced to 50% of the assigned dose if the white blood cell (WBC) count declined to less than 1500/mm^3, the

neutrophil count to less than 750/mm^3, or the platelet (Plt) count to less than 8×10^4/mm^3, and was discontinued if the WBC count declined to less than 1000/mm^3, the neutrophil count to less than 500/mm^3, or the Plat count to less than 5×10^4/mm^3. Ribavirin was also reduced from 1000 to 600 mg, or 800 to 600 mg, or 600 to 400 mg if the hemoglobin (Hb) level decreased to less than 10 g/dl, and was discontinued if the Hb level decreased to less than 8.5 g/dl. Both PEG-IFNα2b and ribavirin had to be discontinued if there was a need to discontinue one of the drugs. During the therapy, ferric medicine or hematopoietic growth factors, such as erythropoietin alpha or granulocyte–macrophage colony-stimulating factor were not administered.

Quantification of HCV RNA and assessment of virological response

Serum HCV RNA titers were quantified using the COBAS AMPLICOR HCV MONITOR Test, version 2.0 (detection range 6–5000 KIU/ml; Roche Diagnostics, Branchburg, NJ, USA) and qualitatively analyzed by the COBAS AMPLICOR HCV Test, version 2.0 (detection threshold 50 IU/ml).

Virological response during and after the therapy was determined according to the American Association for the Study of Liver Diseases (AASLD) practice guideline [17]. The complete early virological responders (c-EVR) were defined as those who showed a reduction in serum HCV RNA quantity to an undetectable level by qualitative PCR at week 12 of the therapy. Virological response was estimated at 24 weeks after cessation of the treatment. Sustained virological response (SVR) was defined as the maintenance of negative serum HCV RNA by PCR for more than 6 months after completion of the therapy. Transient response (TR) was defined as the reappearance of serum HCV RNA within 6 months after cessation of therapy in patients who had achieved negative serum HCV RNA at the end of the treatment. No response (NR) meant that there was persistently positive serum HCV RNA throughout the therapy period. The non-SVR group comprised TR and NR patients.

Assessment of drug exposure

The amounts of PEG-IFNα2b and ribavirin actually taken by patients during the first 12 weeks of the treatment were evaluated by reviewing the medical records as reported previously [18, 19]. The mean doses of both drugs were calculated individually as averages on the basis of body weight at baseline. The dose of PEG-IFNα2b and ribavirin was expressed as micrograms per kilogram per week and milligrams per kilogram per day, respectively.

Analysis of DC subsets, helper T cells, NK cells, and regulatory T cells

For the numerical analyses of blood DC, helper T cells, NK cells, and regulatory T cells (Tregs), venous blood was drawn from patients before treatment and at weeks 8, 12, 24, and 48 during the therapy. Blood samples taken from patients in relevant hospitals were transferred to Osaka University within 6 h and were processed on the same day. Peripheral blood mononuclear cells (PBMCs) were collected by density-gradient centrifugation on a Ficoll-Hypaque cushion. After viable PBMCs had been counted, the cells were stained with combinations of various Abs for phenotypic markers. All immunological assays were performed in Osaka University.

The following monoclonal antibodies were purchased from BD Biosciences (San Jose, CA, USA): anti-Lineage marker [Lin; CD3 (clone SK7), CD14 (clone MφP9), CD16 (clone 3G8), CD19 (clone SJ25C1), CD20 (clone L27), and CD56 (clone NCAM16.2)], anti-CD4 (clone RPA-T4), anti-CD11c (clone B-ly6), anti-CD123 (clone 7G3), anti-CD3 (clone UCHT1), anti-CD45RO (clone UCHL1), anti-CD56 (clone B159), anti-HLA-DR (clone L243), anti-CCR4 (clone 1G1). The antibodies for CD25 (clone B1.49.9) and CD4 (clone 1 3B8.2) were purchased from Beckman Coulter (Fullerton, CA, USA). Anti-CXCR3 (clone 49801) monoclonal antibodies were purchased from R&D Systems (Minneapolis, MN, USA). Staining was performed with FITC, PE, PerCP, and APC conjugated antibodies as described previously [14]. The acquisitions and analyses of data were performed with FACS Calibur (BD Biosciences) and CellQuest software.

Blood DCs were defined as Lin$^-$ and HLA-DR$^+$ cells. Myeloid DCs (MDC) are Lin$^-$, HLA-DR$^+$, CD11c$^+$, and CD123^{low} cells, and plasmacytoid DCs (PDC) are Lin$^-$, HLA-DR$^+$, CD11c$^-$, and CD123^{high} cells. Helper T cell subpopulations were defined by the pattern of CXCR3 and CCR4; Th1 cells are CD4$^+$, CD45RO$^+$, and CXCR3$^+$, and Th2 cells are CD4$^+$, CD45RO$^+$, and CCR4$^+$. NK cells were defined as CD3$^-$ and CD56$^+$ cells. Regulatory T cells (Tregs) were defined as CD4$^+$, CD25^{high+} cells as reported previously [20]. The percentages of DC subsets and NK cells in PBMCs or Th1, Th2 cells and Tregs in CD4$^+$ T cells were determined by FACS. In order to examine the dynamics of immune cells after initiation of the treatment, we used the ratio of frequencies at each time point to those before the therapy [14].

Allogeneic mixed leukocyte reaction with DC

In some patients, we examined whether the allostimulatory ability of DCs was related to the clinical outcomes. Before, at the end of treatment, and at week 4 after completion of

the treatment, monocyte-derived DCs were generated from PBMC obtained from the patients according to methods reported previously [21]. As controls, monocyte-derived DCs were simultaneously generated from healthy donors. As responder cells in mixed lymphocyte reactions (MLR), naive $CD4^+$ T cells were isolated from PBMC of irrelevant healthy donors by using a naive $CD4^+$ T cell enrichment kit (Stemcell Technologies, Vancouver, BC). Allogeneic MLR with DC was performed as reported previously [21]. In order to compare the ability of DC among patients, we determined the MLR ratio between patients and controls as counts per minute (cpm) of [^{3}H]thymidine incorporated into CD4 T cells at the T cell/DC ratio of 10:1.

Statistical analyses

To analyze the relationship between clinical and immunological data at the baseline and virological response, univariate analysis using the Mann–Whitney *U* test or chi-squared test and multivariate analysis using logistic regression analysis were performed. The significance of trends in values was determined with the Mantel–Haenszel chi-square test. Differences of continuous variables between groups were compared by two-way analysis of variance (ANOVA). A two-railed *P* value less than 0.05 was considered significant. These statistical analyses were performed with SPSS version 15.0 (SPSS Inc. Chicago, IL, USA).

Results

Outcome of the PEG-IFNα2b and ribavirin therapy

In 67 patients who had been treated for 48 weeks, 29 (43%) achieved SVR, 18 (27%) were TR, 17 (25%) were NR, and 3 (4%) were unknown (Fig. 1). The clinical backgrounds of these patients are summarized in Table 1. Among these cohorts, 32 patients were c-EVR and were further categorized into 24 SVR (EVR-SVR group) and 8 TR (EVR-TR group). Of the other 35 patients who were not c-EVR, 5 were SVR, 10 were TR, 17 were NR and 3 were unknown. Details of the therapeutic response in the current study are shown in Fig. 1.

Higher platelet counts and Treg increase are involved in SVR in patients who underwent PEG-IFNα2b and ribavirin therapy

In order to clarify whether the frequency and function of immune cells are involved in the outcomes of the combination therapy, we first compared these parameters between SVR and non-SVR groups. Representative dot plots of the immune cell populations are shown in Fig. 2. The identification and enumeration of immune cells were determined by FACS. The pretreatment percentages of DC in SVR were higher than those in the non-SVR group. However, those of PDC, NK cells, Th1, Th2, Treg, and DC function as judged by MLR were not different between them (Fig. 3).

As for the changes of DC subsets during the therapy, in the SVR group, the frequencies of PDC increased after the

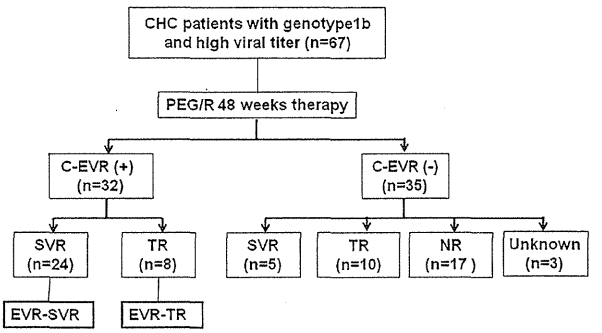

Fig. 1 Detailed outcomes of chronic hepatitis C patients treated with 48-week PEG-IFNα2b and ribavirin combination therapy. In 67 patients who had been treated for 48 weeks, 29 achieved SVR, 18 were TR, 17 were NR, and 3 were unknown. The complete early virological responders (c-EVR) were defined as those who show a reduction in HCV RNA quantity to an undetectable level by qualitative PCR at week 12 of the therapy. According to this criterion, 32 patients were c-EVR and were further categorized into 24 SVR (EVR-SVR) and 8 TR (EVR-TR). Of the other 35 patients who were not c-EVR, 5 were SVR, 10 were TR, 17 were NR, and 3 were unknown. *SVR* sustained virological responder, *TR* transient responder, *NR* non-responder

Table 1 Demographics and clinical backgrounds of the subjects

Factors	Value	Range
Number	67	
Age (years)	51.0 ± 10.3	(24–67)
Gender (M/F)	44/23	
HCV RNA (KIU)[a]	2415	
Activity: A0/1/2/3[b]	0/35/30/1	
Fibrosis: F0/1/2/3/4[b]	2/27/27/9/1	
WBC (/ml)	5229 ± 1299	(2960–9400)
Neutro (/ml)	2663 ± 826	(1077–4516)
Hb (g/dl)	14.6 ± 1.2	(12.0–18.0)
Platelets ($\times 10^4$/mm^3)	16.6 ± 4.6	(5.0–31.0)
ALT (IU/l)	83.1 ± 53.9	(14–269)
T. chol (mg/dl)	172 ± 29	(118–238)
Cr (mg/ml)	0.8 ± 0.2	(0.4–1.3)

All results are expressed as mean ± SD and range

T. chol total serum cholesterol, *Cr* creatinine

[a] Amplicore HCV monitor

[b] Ishak's histological scores

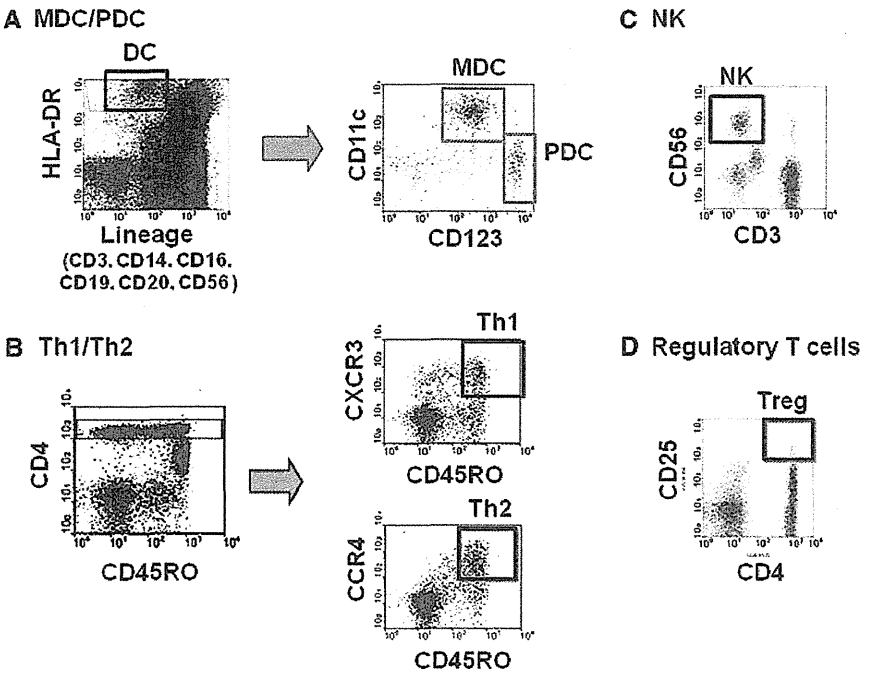

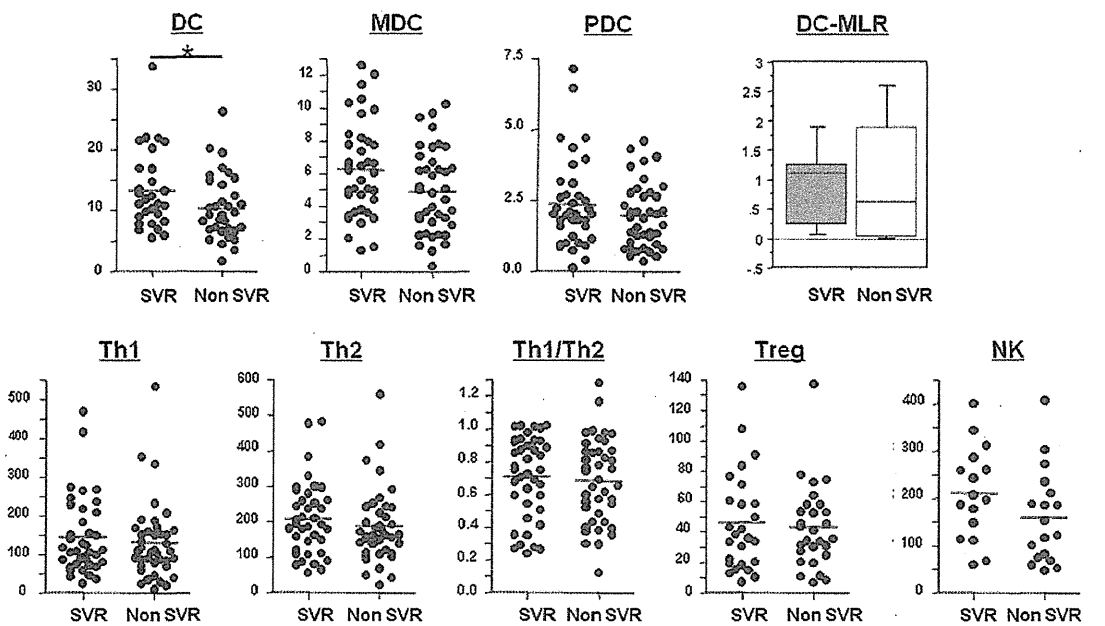

Fig. 2 Phenotypic identification of blood cells by flow cytometry. Representative analyses of myeloid and plasmacytoid dendritic cells (MDC and PDC), type 1 and type 2 helper T cells (Th1 and Th2), natural killer (NK) cells, and regulatory T cells are shown. The combination of surface molecules for the identification of cells is described in "Materials and methods"

Fig. 3 Comparison of pretreatment frequency of blood cells and allostimulatory capacity of monocyte-derived dendritic cells between SVR and non-SVR patients who had been treated with 48-week PEG-IFNα2b and ribavirin therapy. The frequencies of MDC, PDC, Th1 and Th2 cells, Th1/Th2 ratio, NK cells, regulatory T cells, and allogeneic MLR were compared between SVR and non-SVR patients. The MLR ratio between patients and controls was determined from the counts per minute (cpm) of [^{3}H]thymidine incorporated into $CD4^+$ T cells at T cell/DC ratio of 10:1. *$P < 0.05$ by Mann–Whitney U test

beginning of therapy and showed a peak at week 12 of therapy (T12W), which subsided to the end-of-treatment (EOT). Such a PDC increase at the early phase was not observed in the non-SVR group (Fig. 4a). In contrast, the MDC frequency remained at a similar level throughout the therapy, regardless of viral response (data not shown). Alternatively, in the SVR group, the percentages of Treg ($CD4^+CD25^{high+}$ cells) increased through the therapy,

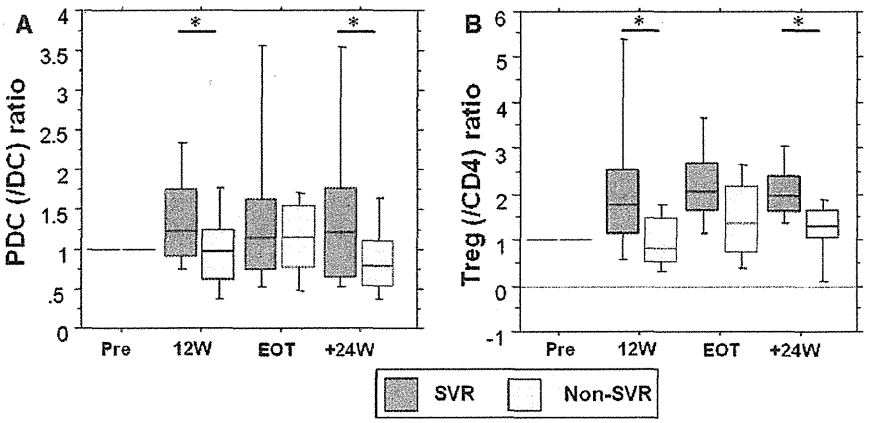

Fig. 4 Changes in frequencies of plasmacytoid dendritic cells and regulatory T cells during and after 48-week PEG-IFNα2b and ribavirin therapy in SVR and non-SVR patients. The ratios of frequencies of PDC (**a**) and Tregs (**b**) at each time point to the pretreatment values were compared between SVR and non-SVR patients. *Boxes* represent lower and upper quartiles, *solid line* within each *box* the median value, *whiskers* the minimum and maximum values. $*P < 0.05$ by Mann–Whitney *U* test. *EOT* end-of-treatment (at 48 weeks of the therapy), *+24W* 24 weeks after the completion of therapy

with cell levels being higher than those in the non-SVR group (Fig. 4b). The other cells, including Th1, Th2, and NK cells, did not differ between the groups (data not shown). Univariate and multivariate analyses were performed to assess the significance of various factors, including demographic, biochemical, virological, immunological parameters, and drug adherence. The allostimulatory capacity of DC after the completion of therapy, whose significance was demonstrated in the previous paper [21], was not included in this study because the numbers of patients examined for it were limited. In univariate analyses, platelet counts, histological activity and fibrosis, dose of PEG-IFNα2b, and attainment of c-EVR were found to be significant in SVR (Table 2). As for immunological markers, pretreatment DC frequency, PDC frequency, their ratio at T12W, and Treg frequency ratio at T12W are significant (Table 3). Based on these parameters, multivariate analysis revealed that platelet counts and Treg frequency at T12W were independent factors involved in SVR (Table 4). These results show that higher platelet counts and Treg increment may be related to SVR in 48 weeks of PEG-IFNα and ribavirin treatment.

Table 2 Univariate analyses of clinical factors involved in SVR

Factors	SVR	Non-SVR
N	29	38
Age (years)	48.0 ± 11.8	53.3 ± 8.6
Gender (M/F)	20/9	24/14
WBC (/mm^3)	5361 ± 1314	5127 ± 1295
Neutro (/mm^3)	2969 ± 861	2461 ± 753
Hb (g/dl)	14.6 ± 1.2	14.5 ± 1.2
Platelets ($\times 10^4$/mm^3)	18.2 ± 4.4*	15.2 ± 4.4
ALT (IU/l)	72 ± 54	92 ± 53
HCV RNA (KIU/ml)	2103	2654
Activity: 0–1/2–3/n.d.	29/0/0$^{\#}$	27/10/1
Fibrosis: 0–2/3–4/n.d.	20/9/0*	15/22/1
PEG-IFN dose (μg/kg/day)	1.43 ± 0.14$^{\#}$	1.31 ± 0.22
Ribavirin dose (mg/kg/day)	10.6 ± 1.5	9.9 ± 1.4
c-EVR: +/−	24/5$^{\#}$	8/27

Mann–Whitney *U* test, chi-square test

n.d. not determined

$*P < 0.05$, $^{\#}P < 0.01$

Higher platelet counts and PDC increase are independent factors involved in SVR after attainment of c-EVR

Next, we examined the above-mentioned immunological parameters in patients who attained c-EVR, as they were considered to be comparable with respect to the virological response to the therapy. Among 32 patients in the c-EVR group, 24 developed to SVR (EVR-SVR) and the remaining 8 to TR (EVR-TR) (Fig. 1). Univariate analysis disclosed that lower age is a characteristic of the EVR-SVR patients compared with those in the EVR-TR group (Table 5). As for immunological markers, pretreatment DC frequency, PDC frequency, and PDC ratio at T12W were higher in EVR-SVR patients than those in EVR-TR (Table 6). The pretreatment percentages of MDC, PDC, Th1, Th2, NK cells, and Tregs and those at any all points during the therapy did not differ between EVR-SVR and EVR-TR patients (data not shown). Multivariate analyses revealed that higher platelet counts and PDC increase at T12W were independent factors involved in EVR-SVR (Table 7). These results indicate that the dynamics of PDC